Ministry of Education and Science of Ukraine
Ternopil Ivan Puluj National Technical University

Faculty of Applied Information Technologies and Electrical Engineering
(full name of faculty)
Electrical Engineering
(full name of department)

QUALIFYING PAPER

For the degree of

bachelor
(degree name)

topic: **CALCULATING THE PARAMETERS OF AN ELECTRIC MOTOR BASED ON ITS MODEL**

Submitted by: fourth year student 4 , group IET-43
specialty
141 Electrical Engineering
(code and name of specialty)

	(signature)	Arthur MWABA NKUNKA (surname and initials)
Supervisor	(signature)	Koval V.P. (surname and initials)
Standards verified by	(signature)	Koval V.P. (surname and initials)
Head of Department	(signature)	Koval V.P. (surname and initials)
Reviewer	(signature)	Savkiv V.B. (surname and initials)

Ternopil 2025

Ministry of Education and Science of Ukraine
Ternopil Ivan Puluj National Technical University

Faculty Faculty of Applied Information Technology and Electrical Engineering
(full name of faculty)
Department Electrical Engineering
(full name of department)

APPROVED BY
Head of Department
____________ Vadym KOVAL
(signature) (surname and initials)
« 12 » 12 2024

ASSIGNMENT
FOR QUALIFYING PAPER

for the degree of Bachelor
(degree name)
specialty 141 Electrical Power Engineering, Electrical Engineering and Electromechanics
(code and name of the specialty)
student *Arthur MWABA NKUNKA*
(surname, name, patronymic)

1. Paper topic *Calculating the parameters of an electric motor based on its model*

Paper supervisor *Koval Vadym Petrovich, Ph.D., Head of Department EE*
(**surname, name, patronymic**, scientific degree, academic rank)
Approved by university order as of «*12*» *12* 2024 № *4/7-1169*
2. Student's paper submission deadline 24.01.2025
3. Initial data for the paper

4. Paper contents (list of issues to be developed)
1. Analysis and classification of AC motors
2. Choosing a method for calculating the electric and thermal fields of electric motors
3. Preliminary calculation of electric motor parameters
4. Calculation of losses
5. Temperature calculation of the electric motor

5. List of graphic material (with exact number of required drawings, slides)
1. Core of the stator magnetic circuit
2. Design of magnetic circuit and winding of a short-circuited rotor
3. Asynchronous motor
4. Dependence of air thermal conductivity on temperature
5. Calculation errors of the temperature exceedance of the thermodynamic model components in steady-state mode
6. Finite element mesh of the electric motor model

6. Advisors of paper chapters

Chapter	Advisor's surname, initials and position	Signature, date	
		assignment was given by	assignment was received by
Labour occupational safety	*Ph.D., Assistant professor Okipnij I.B.*		
and security in emergency			
situations			

7. Date of receiving the assignment *12.12.2024*

TIME SCHEDULE

LN	Paper stages	Paper stages deadlines	**Notes**
1	Preparation of the « ANALYTICAL PART »	01.01.25 – 05.01.25	
2	Preparation of the « DESIGN AND DEVELOPMENT	05.01.25 – 12.01.25	
	SECTION»		
3	Preparation of the « CALCULATION SECTION »	12.01.25 – 20.01.25	
4	Preparation of the «LABOUR OCCUPATIONAL	20.01.25 – 22.01.25	
	SAFETY AND SECURITY IN EMERGENCY		
	SITUATIONS»		
5	Preparation of introduction, conclusions,	22.01.25 – 24.01.24	
	Content and summary.		
6	Preparation, execution and printing graphic material of	22.01.25 – 24.01.25	
	thesis		
7	Getting feedback and review of thesis	22.01.25 – 24.01.25	
	And drafting a report for the defense.		

Student ____________ *Arthur Mwaba Nkunka*
(signature) (surname and initials)

Paper supervisor ____________ *Koval Vadym Petrovich*
(signature) (surname and initials)

ABSTRACT

Bachelor's thesis. Ternopil Ivan Puluj National Technical University. Faculty of Applied Information Technologies and Electrical Engineering.

Department of Electrical Engineering, IET-43 group. - T.: TNTU, 2025.

The qualifying work of the bachelor was performed on the basis of the task on the topic: " Calculating the parameters of an electric motor based on its model ".

The mathematical models for calculating electromagnetic and thermal fields are presented, which allow determining losses in motors and temperatures of its elements, both in the stationary and transient processes.

The analysis shows the importance of taking into account the temperature change in winding resistance when constructing thermodynamic models of electric machines. It is shown that the change in the winding temperature will be insignificant within the cycle, but the average temperature level of the model nodes will significantly depend on the fact of taking into account the temperature change in resistance

Keywords: mathematical models, electric motor, temperature.

CONTENTS

INTRODUCTION

Electric motors are an integral part of the technological progress of modern society. They are widely used in production, households, technological processes and mechanisms. One of the most common types of AC electric motors is the induction motor. The simplicity and cost-effectiveness of its design makes this type of electric motor reliable for wide application in many industries.

Being widely used, this type of electric motor must be energy efficient to meet the ever-growing demand for electricity. In order to design and build an efficient motor, it is very important to have in-depth knowledge of the losses occurring in the machine.

Currently, one of the challenges in electromechanics is the accuracy of estimating and calculating electric machines for heating and heat generation. Moreover, this task needs to be solved at the initial stage.

It is the level of thermal loads that determines the limit for the insulation of winding wires, bearing assemblies, and other areas, limiting the motor's service life. The thermal field assessment makes it possible to make the necessary changes to the motor parameters and is relevant at the design stage to optimize its design with the required output characteristics, conditions, and operating time.

The analysis of existing methods for calculating electromagnetic and temperature fields of induction motors, as well as other electrical products, revealed the existence of different ways to calculate them using the method of equivalent circuits and the numerical method, which showed the required accuracy. To achieve the most accurate result, it is necessary to take into account as many factors as possible that contribute to the appearance of losses, heating/cooling, and to consider the thermal field in dynamics.

Purpose and objectives of the study. The purpose of the thesis is to calculate the electrical and temperature characteristics of an AC motor based on its mathematical model.

In order to achieve this goal, the following tasks were solved in the work:

1. To consider the current state of the theory of calculation and modeling of thermal processes in electric machines.

2. To develop a mathematical model of an induction motor that allows obtaining results in a short time by changing the input data, dimensions, and properties of its structural elements.

3.To simulate the thermal modes of an induction motor with the determination of electromagnetic and temperature fields and the level of losses in the main structural components.

1 ANALYTICAL PART

1.1 Analysis and classification of AC motors

An electric motor is a device for converting electricity into rotational motion of a rotating part of an electric machine. Energy conversion in motors occurs due to the interaction of the magnetic fields of the stator and rotor windings. These electric machines are widely used in all industries as a drive for electric vehicles and tools, in automation systems, household appliances, and so on.

There are many types of electric motors that differ in terms of their principle of operation, design, performance, and other features.[1] Let's consider the main types of these electric machines.

According to the principle of operation, there are magnetoelectric and hysteresis electric machines. Despite their simple design and high starting torque, the latter are not widely used. These electric motors have a high price and low power factor, which limit their use. The vast majority of electric motors are magnetoelectric.

Electric motors with horizontal and vertical shafts are distinguished by design. In addition, electric machines are classified by purpose, climate design, degree of protection against moisture and foreign objects, power, and other parameters.

AC motors can be divided into two categories^ asynchronous and synchronous.[2-3]

1.2 Asynchronous electric motors

Due to their cheapness and simplicity of design, electric machines of this type are the most widespread. Their fundamental difference is the presence of the so-called slip. This is the difference between the rotational speed of the magnetic field of the stationary part of the electric machine and the speed of the rotation rotor. The voltage on the rotating part is induced by the alternating magnetic field of the motor stator windings. Rotation causes the interaction of the field of electromagnets of the stationary part and the magnetic field of the rotor, which arises under the influence of eddy currents induced in it. According to the characteristics of the stator windings, there are:

– Single-phase AC motors. Motors of this type require an external phase-shifting element to start. This can be a starting capacitor or an inductive device.

– Two-phase electric machines. Such motors have two windings with phases shifted relative to each other.

– Three- and multi-phase electric motors. The most common type of induction machines. Electric motors of this type have 3 or more stator windings shifted in phase by a certain angle.

According to the rotor design, induction electric machines are divided into squirrel-cage and phase rotor motors.

The rotor winding of electric machines of the first type consists of several non-insulated rods made of copper or aluminum alloys, closed on both sides with rings (squirrel cage design). Asynchronous motors of this type have the following advantages:

– A fairly simple start-up scheme. Such electric machines can be connected directly to the mains via switching devices.

– Allowance for short-term overloads.

– The ability to manufacture high-power electric machines. This type of motor does not contain sliding contacts that impede power growth.

– Relatively easy to repair. Asynchronous electric machines are lightweight.

– Low price. Asynchronous motors are cheaper than synchronous machines and DPS.

Electric machines with a short-circuited rotor have disadvantages:

– The maximum rotational speed does not exceed 3000 rpm when entering synchronous mode.

– Technically complex implementation of speed control.

– High inrush currents during direct start-up.

Electric motors with a phase rotor are partially free from the disadvantages inherent in machines with a squirrel-cage rotor. The rotating part of an electric machine of this type has windings connected in a “star” pattern. The voltage is supplied to the winding through 3 slip rings attached to the rotor and isolated from it.

Such electric motors have the following advantages:

– The ability to limit inrush currents using a resistor connected to the rotor electromagnet circuit.

– Higher starting torque than squirrel-cage motors.

– The ability to adjust the speed.

– Constant rotational speed under variable load.

– High efficiency and power factor.

– A small reactive component.

– Overload tolerance.

The disadvantages of synchronous motors include:

– High price, relatively complex design.

– Difficult launch.

– The need for a constant voltage source.

Difficulty controlling the rotational speed and shaft torque.

All the disadvantages of AC electric machines can be corrected by installing a soft-start device or a frequency converter. The rationale for choosing a particular device is based on economic feasibility and the required characteristics of the electric drive.

1.3 Design analysis of induction motors

An induction motor consists of two main parts separated by an air gap: a stationary stator, which is basically an inductor, and a rotating rotor. The stator and rotor consist of a core - a magnetic core with grooves and windings.

The main structural components of the induction motor shown in Figure 1.1 include a slotted magnetic core of the stator with an AC winding pressed into the frame; slotted magnetic core of the rotor with a winding mounted on a rotating shaft that transmits electromagnetic torque to the load; bearing units; bearing shields; fan; terminal box; and a device for attaching to the foundation or base.

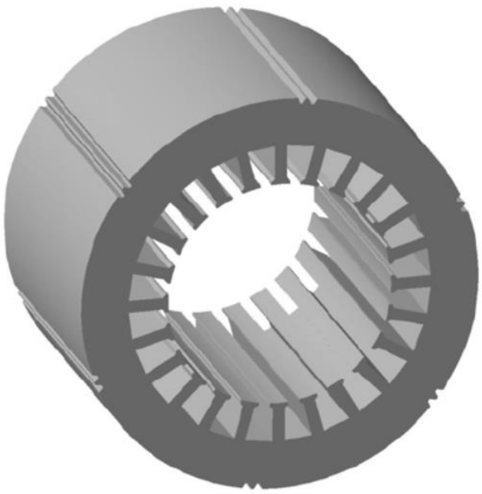

Figure. 1.1 - Core of the stator magnetic circuit without winding

There are two main types of induction motors: squirrel-cage motors and split-rotor motors. Both motors have the same stator design and differ only in the rotor design.

In terms of mounting method, the most common are IM1 through IM4 versions. Among the low-power machines, IM5 and IM9 versions are common, which are used in household appliances and electrified tools.

In terms of environmental protection, IP44 and IP54 versions with IC041 cooling method are common for low-power machines, and IP23 version with IC01 cooling method is also common for medium and high-power machines.

The magnetic core of the stator core is made of 0.35-0.5 mm thick electrical steel sheets. The stator core of an induction motor with an axis height of h ≤ 250 mm is assembled from the tinned sheets of electrical steel with the inner diameter and slotting based on the slots. If steel grade 2013 is used, the sheets undergo heat treatment after stamping and subsequent oxidation in automatic furnaces. The assembled core is compressed under a pressure of ≈1.5 mPa and fastened with steel staples placed on the outer surface of the core.Motor cores h = 50-90 mm are welded from the outer surface. The wrapped and impregnated motor stator cores are pressed into the frame. Sometimes the magnetic core sheets are installed directly into the frame and, during the pressing process, are secured with ring dowels or gathered onto a centering mandrel outside the frame and steel strips located in shallow rectangular grooves welded to the pressure washers and partially to the back of the core.

The shape of the core grooves is mainly trapezoidal semi-closed; rectangular open. The designs of induction motor frames with IP44 and IP23 protection ratings are fundamentally different. The frame of an IP44 motor with h ≤ 355 mm is made in the form of a cylinder with longitudinal ribs on the outer surface (Fig. 2) or with air cooler tubes for motors with h > 400 mm.

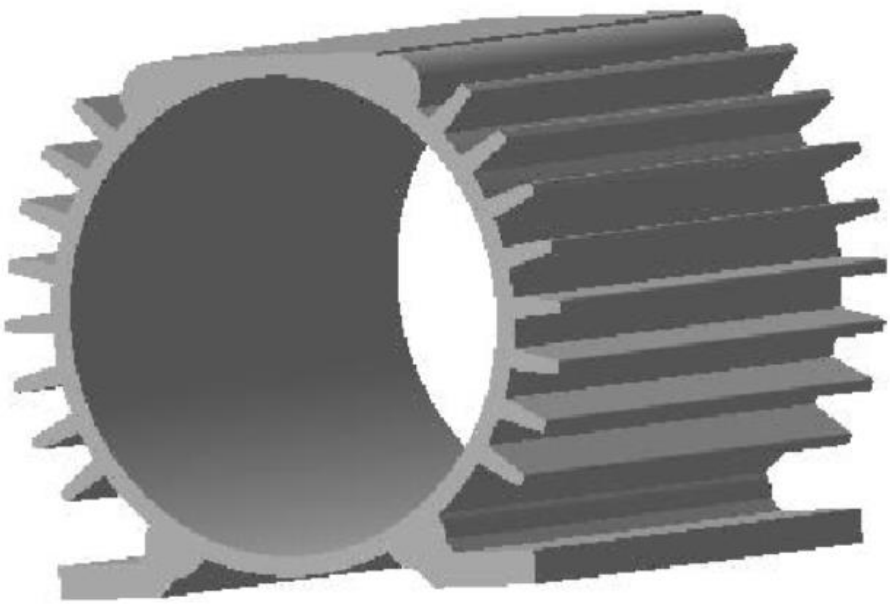

Figure 1.2. - AD frame in IP44 version

For motors with $h < 63$ mm, the frames are cast from aluminum. For $h = 71$-100 mm, a combined design is used: aluminum alloy frames and cast iron bearing plates.

The method of making frames from a hollow profile obtained by extruding an aluminum alloy in the form of a pipe is becoming increasingly common.

Asynchronous motors with cast iron shells (frames) up to $h \leq 280$ mm are the most widely used in the world's electrical engineering practice. Motors with $h > 280$ mm are made with welded steel frames.

By design, the rotor of an induction motor is made of a short-circuited squirrel-cage type (Fig. 1. 3) or a phase rotor, in the grooves of which an alternating current winding is placed, having the same number of phases and poles as the stator winding.

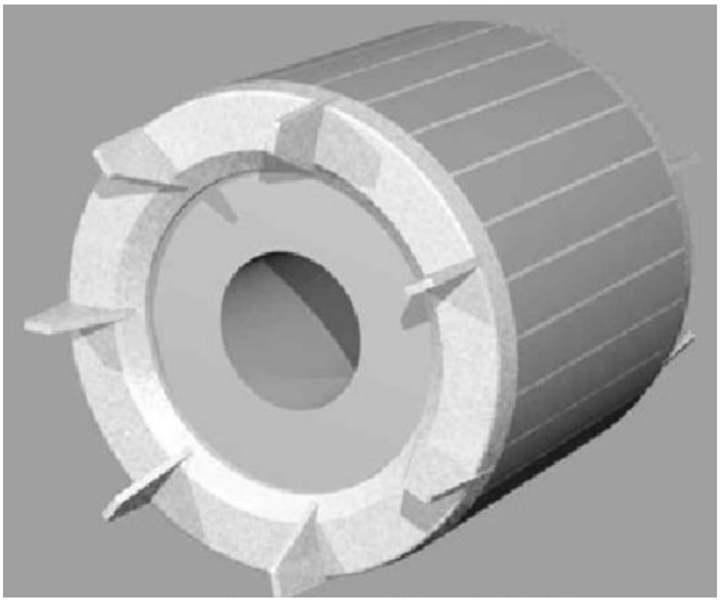

Figure 1.3 - Short-circuited rotor

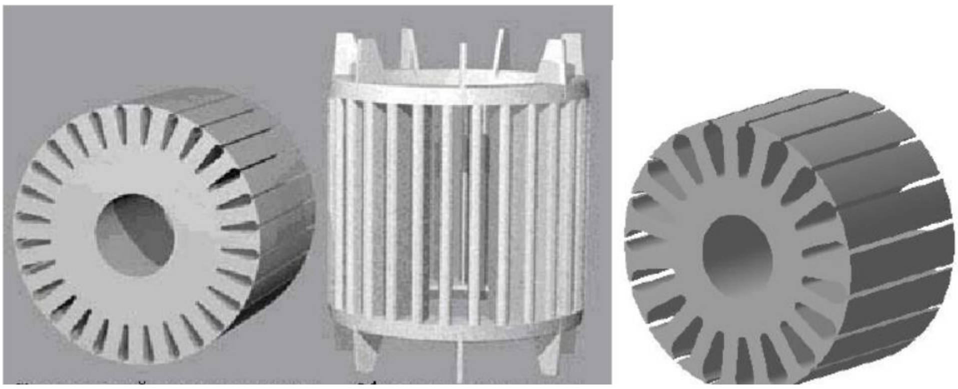

Figure 1.4 - Design of magnetic circuit and winding of a short-circuited rotor

The rotor consists of a magnetic core and a squirrel-cage short-circuited winding (Fig. 1.4).

The rotor and winding are pressed onto the motor shaft. The rotor core sheets are stamped simultaneously with the stator sheets.

Rotor sheets for motors h < 250 mm are made of steel 2013 and are collected on a mandrel, pressed and fixed on the mandrel without pressure release. In this form, the rotor core is filled with aluminum.

The cores of squirrel-cage rotors are pressed onto the shaft after being filled with aluminum. During the aluminum casting process, the short-circuit rings and ventilation blades are formed simultaneously.

The phase rotor consists of a magnetic core and a belt current winding, the phases of which are connected in a star, less often in a triangle, and have three leads that are connected to slip rings located inside the housing or at the protruding end of the shaft.

1.4 Analysis of ways to improve the energy efficiency of electric motors

The issue of creating energy-saving electric motors arose simultaneously with the invention of electric machines themselves. At the International Electrical Exhibition in 1891 in Frankfurt am Main, Charles Brown (who later founded ABB) showed a synchronous three-phase generator of his own production, the efficiency of which exceeded 95%. The asynchronous three-phase motor presented by Mikhail Dolivo-Dobrovolsky showed an efficiency of 95%. Since then, the efficiency of the three-phase induction motor has been improved by only one or two percent. The interest in energy-saving motors was most acute in the late 1970-x years during the global oil energy crisis. It turned out that saving one ton of conventional fuel is much cheaper than producing it. During the crisis, investments in energy saving increased many times over. Many countries began to allocate special grants for energy saving programs.

After analyzing the problem of energy saving, it turned out that more than half of the electricity produced in the world is consumed by electric motors. Therefore, all the world's leading electrical engineering companies are working to improve them.

- The increase in efficiency in energy-saving motors is achieved by:
- Increasing the share of active materials - copper and steel;
- Use of thinner and higher quality electrical steel;
- Use of copper in rotor windings instead of aluminum;
- Reducing the air gap in the stator with the help of precision process equipment;
- Optimization of the shape of the magnetic circuit tooth zone and winding design;
- Use of bearings of the highest class;
- Special fan design;

According to statistics, the price of the entire motor is less than 2% of the total life cycle costs. For example, if the motor operates 4000 hours annually for 10 years, electricity accounts for approximately 97% of the total life cycle costs. Another one percent is accounted for by installation and maintenance. Therefore, a 2% increase in the efficiency of a medium-power motor will pay for the increased cost of an energy-saving motor in as little as 3 years, depending on the operating mode. Practical experience and calculations show that the increase in the cost of an energy-saving motor pays for itself through the saved electricity when operating in S1 mode in a year and a half (with an annual operating time of 7000 hours).

A negative property of electric motors with increased efficiency compared to conventional motors is:

- 10-30% higher cost;
- slightly higher mass;

– higher starting current.

The amount of energy savings due to the introduction of an energy-efficient motor may be insignificant compared to the potential of a drive with variable speed. Each additional percentage point of efficiency requires an increase in the mass of active materials by 3-6%. At the same time, the rotor moment of inertia increases by 20-50%. Therefore, high-efficiency motors are inferior to conventional motors in terms of dynamic performance unless this requirement is specifically taken into account when designing them.

When choosing in favor of an energy-efficient motor, you need to carefully consider the price. Analysts predict that copper will rise in price much faster than steel. Permanent magnets made of rare earth materials will rise in price more and faster than copper, which will lead to a significant increase in the price of such motors. That is, a motor with a higher content of these materials will be more expensive when it is replaced at the end of its service life.

2 DESIGN AND DEVELOPMENT SECTION

2.1 Choosing a method for calculating the electric and thermal fields of electric motors

There are two approaches to analyzing electrical machines: using the methods of circuit theory and field theory.

Thanks to the methods of circuit theory, it was possible to build a very rigorous and understandable classical theory of electric machines, as well as to obtain their substitution schemes. However, the use of circuit theory methods to take into account the peculiarities of the electric machine design and to solve overly complicated systems of equations describing nonlinear processes proved to be inconvenient and not always possible.

The use of methods based on field theory made it possible to eliminate the disadvantages of circuit theory methods due to the possibility of finding field values (magnetic, thermal, and other fields) at any point in the volume of an electric machine, as well as to obtain a complete picture of the distribution of these values in different parts of the electric machine with the subsequent finding of integral values. Among the field calculation methods, analytical and numerical methods are the most common.The advantage of analytical calculation methods is the possibility of a rigorous mathematical description of phenomena as algebraic or differential equations, allowing to analyze the dependence of field values on the initial parameters, to establish an accurate relationship between different values. However, a rigorous analytical description is possible only for relatively simple models with assumptions that in some cases can lead to unacceptable errors.

Numerous methods for calculating the field can eliminate these shortcomings. In the absence of the need for a strict mathematical description of the processes occurring in an electric machine, the use of numerical methods is preferable, since in this case the assumptions made in the calculation of the fields are minimal, and the calculation error is determined by only by the size of the computational grid used. Among the known numerical methods field calculation The main one is the finite element method (FEM). Compared to the finite difference method, the FEM is convenient to use for models of a rather complex configuration and with different mesh densities.

Among all the variety of modern computational tools, we highlight the most common software packages, such as ANSYS multiphysics, Maxwell, Comsol multiphysics, Flux, Jmag, FEMM, which allow solving many, including related field problems: electromagnetic, thermal, mechanical stress field, taking into account their mutual influence. For some tasks, the capabilities of software systems may be excessive. For example, to calculate cylindrical machines, it is often sufficient to solve a two-dimensional problem assuming a plane-parallel magnetic field. The validity of this approach is well known. In this case, the computational time is reduced several times, and the error is acceptable for engineering problems. [6]

Modeling of the magnetic field is always accompanied by a number of assumptions, each of which makes the model to some extent different from the real object. In terms of saving computational time, it is advantageous to use simpler models. However, the accuracy of the result may be unacceptably low. Therefore, in this paper, we have chosen the position of minimizing the assumptions made, as well as building a model that is closest to the actual geometry and parameters of the electric machine.

2.2 Methods for modeling electrical processes in the stator winding

The study of current displacement in rectangular conductors of a compact winding is associated with solving the problem of modeling the magnetic field generated by alternating three-phase currents of the winding stator in the cross-section of the active part of the machine.

The finite element method allows us to accurately take into account the influence of the design features of the compact winding on the electrical in the winding, and to propose a refined method for calculating the active resistance of the winding phase of the stator. To obtain a picture of the current density distribution, the Laplace differential equation is solved with respect to the electric potential φ. In general, for a three-dimensional problem in the case of an isotropic conductor, the partial differential current equation with the Dirichlet boundary condition is as follows:

$$-j=\frac{\partial}{\partial x}\left(\gamma\frac{\partial\varphi}{\partial x}\right)+\frac{\partial}{\partial y}\left(\gamma\frac{\partial\varphi}{\partial y}\right)+\frac{\partial}{\partial z}\left(\gamma\frac{\partial\varphi}{\partial z}\right) \tag{0.1}$$

For magnetostatics, the problem of current distribution in the volume of a conductor is transformed into the problem of electric potential distribution. The need to study the current flow in the volume of a conductor of variable cross-section of a compact winding arises not only when the conductor cross-section changes, but also when the depth of current penetration changes due to the surface effect. In finite element analysis software packages, systems of Laplace's differential equations are solved to numerically determine the field values. For a two-dimensional problem, the solution to the problem of current distribution in the volume of the conductor is defined as:

$$-j=\frac{\partial}{\partial x}\left(\gamma\frac{\partial\varphi}{\partial x}\right)+\frac{\partial}{\partial y}\left(\gamma\frac{\partial\varphi}{\partial y}\right) \tag{0.2}$$

From Equations 2.1 and 2.2, it follows that the calculation of the Laplace equation in a two-dimensional formulation allows to reduce the number of calculations compared to the three-dimensional model.

Traditional methods of designing AC electric machines study the effect of current displacement mainly in the asynchronous rotors of short-circuited machines. Under starting conditions, current displacement to the air gap occurs in the rods of the squirrel cage, and therefore the rotor winding is made with deep rods to increase the starting torque of the induction motor. However, the effect of uneven current distribution in traditional stator windings is not taken into account.The model assumes that the processes in the stator volume repeat cyclically both in space and time, which allows the following differential equations to be used to describe the distribution of the thermal field.

The finite element method is conveniently used to calculate the electromagnetic field and heat sources of induction motors. For a two-dimensional plane model, the field is described by Eq:

$$j\omega\sigma A+\nabla\times(\mu_0^{-1}\mu_r^{-1}\times A)-\sigma v\times(\nabla\times A)=\left(\frac{\sigma\Delta V}{L}+J_Z^e\right)e_Z A=A_z e_Z \qquad (0.3)$$

J_Z^e - density of the external current;

v - velocity vector of the rotor elements;

σ - electrical conductivity;

A - vector magnetic potential;

μ_0 - magnetic permeability of the vacuum;

μ_r - relative magnetic permeability of the medium;

ΔV - potential difference applied to the conductor;

L - length of the conductor in the direction of the Z-axis;

ω - circular frequency.

As boundary conditions, we assume that the magnetic potential at the remote boundary of the computational domain is equal to zero:

$$A_Z = 0 \qquad (0.4)$$

One of the tasks in the design of alternating current machines is to calculate the limit modes to ensure the permissible temperature of the current-carrying parts and cores of the stator and rotor [7-9]. To determine internal heat sources, the electromagnetic problem in the rotor and stator conductor system is first solved. In the active conductors of the rotor, depending on the slip, the current frequency changes, which leads to a redistribution of losses in these conductors. The problem of determining the heat sources in the conductors of the winding frontal parts is considered separately. The absence of a closed magnetic circuit in the space near the winding faces leads to a current density distribution pattern that differs from the current distribution in active conductors. Even at low current frequencies, an uneven distribution of current density is observed in certain sections of the daiquiri windings. current density and, more importantly, in the distribution of the power density of heat generation.

2.3 Methodology for modeling losses in electric motors

Steel losses are divided into two main components: magnetization losses and eddy currents. They depend on the steel grade, thickness of the magnetic circuit sheets, magnetization frequency, and induction. They are also affected by various technological factors. The process of stamping magnetic circuit sheets produces a flake that changes the structure of the steel along the edges of the teeth and increases hysteresis losses. Eddy current losses increase as a result of short circuits of some magnetic circuit sheets among themselves, which arise due to burrs formed during the sawing of grooves, when groove wedges are hammered, due to excessive pressing of the magnetic circuit and a number of other reasons [12, 13]. To combat eddy currents, magnetic circuit structures are used that are shimmed in the direction of eddy current flow. Accounting for losses in such a magnetic circuit design is a non-trivial task.

In engineering practice, the semi-empirical formula is used to determine the magnetization and eddy current losses with a sinusoidal magnetic flux curve

$$\Delta P_{cm} = k_m \left(\frac{\Delta P_{nm}}{m} \right)_{1/50} B^2 \left(\frac{f}{50} \right)^{\beta} m_c, \tag{0.5}$$

were k_m – a correction factor that takes into account the increase in losses caused by the technological process of core assembly, it is recommended to take a correction factor from the range k_m = 1,4–2 depending on the machine power, the geometry of the steel parts (teeth, yoke), etc;

$\left(\frac{\Delta P_{nm}}{m}\right)_{1/50}$ – specific steel losses per unit mass at 1 T induction and frequency 50 Hz;

B – is the amplitude value of induction;

f – frequency;

m_c – core mass.

Equation (2.3) is based on a simplified engineering approach that does not include the division of losses into eddy current losses and hysteresis.

The main losses in steel in induction motors are calculated only in the stator core, since the rotor magnetization frequency equal to $f_2 = sf_1$ (s - sliding, f_1 - network frequency) in close to nominal modes is very small and losses in the rotor steel are negligible even at high inductions.In addition, engineering calculations also use an approach based on the Steinmetz equation [14]

$$\Delta P_{cm} = \Delta P_h + \Delta P_e = k_h f^{\beta} + k_e f^2 B^2, \qquad (0.6)$$

were ΔP_h – magnetization losses;

ΔP_e – eddy current losses;

α , β - empirical coefficients (usually not integer) α, β lie within the range 2 < α < 3, 1 < β < 3;

k_h – is the correction factor for hysteresis losses,

k_e - correction factor for eddy current losses.

Calculations and experimental data show a significant increase in losses with a non-sinusoidal magnetic flux and significant saturation of the magnetic system, etc.

To take into account these additional factors that significantly affect the result, Equation (2.6) is supplemented by a third term, the so-called additional (excess) losses:

$$\Delta P_{cm} = \Delta P_h + \Delta P_e + \Delta P_{ex} = k_h f^{\beta} + k_e f^2 B^2 + k_{ex} f^{1.5} B^{1.5} \tag{0.7}$$

were k_{ex} - correction factor for additional losses.

The energy consumed for magnetization is most often determined by the area of the quasi-static hysteresis loop (Sh) and, for f cycles at the specific density of the material, can be found by the formula

$$\Delta P_h = \frac{f}{4\pi\gamma} \oint B dH = \frac{S_h f}{4\pi\gamma}. \tag{0.8}$$

The correction factor for eddy current losses can be calculated for a material with a resistivity and sheet thickness Δst using the following formula:

$$k_e = \frac{(\pi \Delta_{cm})^2}{6\rho\gamma}. \tag{0.9}$$

The correction factor for hysteresis losses can be defined as

$$k_h = \frac{\Delta p_{cm}}{B^2 m f} - \frac{\pi^2 \Delta_{cm}^2 f}{6\rho\gamma}, \tag{0.10}$$

were Δp_{cm} - specific steel losses (Wt/кг).

Accurate determination of losses by analytical methods is difficult due to the complex distribution of magnetic induction across the machine cross-section. Numerical modeling allows us to specify the magnitude and localization of these losses.

2.4 Heat sources in electric motors

The conversion of electrical energy in electromechanical converters is accompanied by irreversible heat losses. From the point of view of thermal stress, the most vulnerable part of electrical machines and apparatus is insulation. When the permissible temperature value is exceeded, the insulation changes its structure, as a result of which its aging is more intense and, with a further increase in temperature, the insulation is completely destroyed, which can lead to a short circuit and an emergency. Materials used as insulating materials are divided into several groups depending on the maximum permissible temperature exceedance.[8] Heat sources are the active structural elements - windings and, to a lesser extent, rotor and stator magnetic cores - and the outer surface of the machine casing is the sink. From the point of view of the thermal state of the machine, let's consider a segment of an induction machine containing one stator slot and one rotor slot (pic. 2.1).

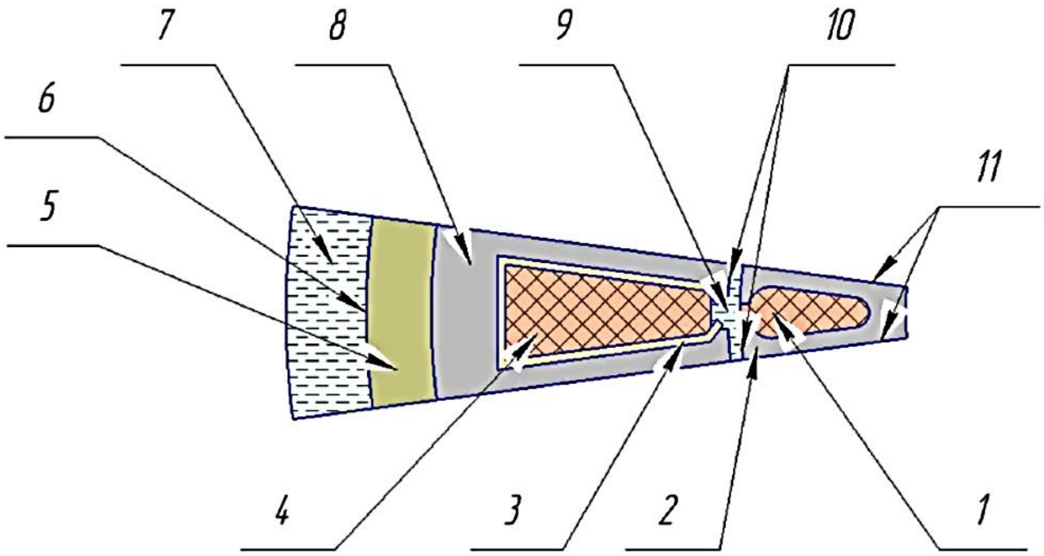

Figure 2.1 - Asynchronous motor segment:
1 – rotor winding; 2 - rotor magnetic circuit; 3 - stator groove insulation; 4 - stator winding; 5 - machine body; 6 - outer surface of the body; 7 - surrounding air; 8 - stator magnetic circuit; 9 - air gap; 10 - gap limiting surface; 11 - symmetry surfaces

All the grooves are in identical thermal conditions. Let us assume that the heat flow in the middle section of the machine is directed only in the radial direction - from the rotor groove into the gap and from the stator groove to the housing and then to the environment. Axial heat dissipation through the shaft and rotor grooves is neglected.

The main internal sources of heat in an electric machine are electrical losses in the windings and losses in the steel of the stator magnetic circuit.

Electrical losses в m_1-of the stator phase winding are determined by the active resistance of the winding phase R1 and the square of the current value I_1 [12, 13]:

$$\Delta p_{ф} = m_1 I_l^2 R_l \tag{0.11}$$

When modeling thermal processes, it is more convenient to use losses calculated based on the cross-section of the winding slots:

$$p_{nm} = I^2 R = j^2 q^2 \rho \frac{l}{q} = j^2 qpl = \rho j^2 l_\delta S k_s, \tag{0.12}$$

were ρ – resistivity of the wire material at operating temperature, Ω·m;

j – current density, A/m^2;

q – conductor cross section, m^2;

l_δ - length of the conductor in the groove, m;

S – the area of the grooves, m^2;

k_s – coefficient of groove filling with copper.

To solve the heat field problem, the heat sources are given by the volumetric density of heat emission Q, Wt/m^3, therefore, the losses calculated by formula 2.12 should be divided by the volume V, which is the source of heat generation.

$$Q = \frac{P}{V} = \frac{\rho j^2 k_3 l_\delta S}{l_\delta S} = \rho j^2 k_3, \tag{0.13}$$

The main magnetic losses of induction motor steel can be determined by the following relations (2.7)–(2.13).

2.5 Thermal calculation of electric machines based on numerical calculation methods

The method of thermal calculation of an electric machine is usually based on solutions to the heat conduction equation. Since energy losses are released inside the structural elements of an electric machine, its temperature field is a field with internal heat sources, and the thermal conductivity equation describing this field is a nonhomogeneous equation [9-10].

The derivation of the differential equation of thermal conductivity is based on the law of energy conservation, which in the case under consideration can be formulated as follows: the amount of heat introduced into an elementary volume from the outside during time due to thermal conductivity, as well as from internal sources, is equal to the change in the internal energy or enthalpy of the substance contained in the elementary volume:

$$dQ_1 + dQ_2 = dQ \tag{0.14}$$

де dQ_1 — is the amount of heat [J] introduced into an elementary volume by heat conduction during time dt;

dQ_2 — is the amount of heat that has been released in an elementary volume over time due to internal sources; dQ — The change in the internal energy contained in an elementary volume over time .The amount of heat supplied by heat conduction to the volume under consideration is equal to:

$$dQ_1 = -\left(\frac{\partial q_x}{\partial t} + \frac{\partial q_y}{\partial t} + \frac{\partial q_z}{\partial t} \right) dxdydzdt, \tag{0.15}$$

The distribution of heat flows is shown in the figure 2.2.

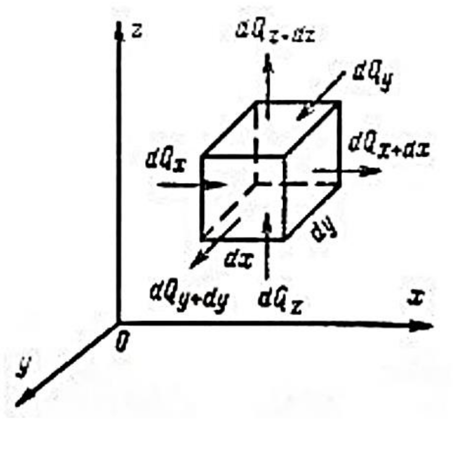

Figure 2.2 - Volumetric propagation of heat fluxes

The second component of equation (2.14):

$$dQ_2 = q_1 d\vartheta dt, \tag{0.16}$$

were q_1 - power of internal heat sources, [Wt/m^3].

The third term of the equation (2.14):

$$dQ = C_V \frac{\partial T}{\partial t} dt d\vartheta = c_V \rho \frac{\partial T}{\partial t} dt d\vartheta, \tag{0.17}$$

were C_V - heat capacity per unit volume, (m3·K), c_V - heat capacity per unit mass, J/(kg-K); - density of a substance.

$$c_V \rho \frac{\partial T}{\partial t} = -\left(\frac{\partial q_x}{\partial x} + \frac{\partial q_y}{\partial y} + \frac{\partial q_z}{\partial z} \right), \tag{0.18}$$

$$c_V \rho \frac{\partial T}{\partial t} = -div\overline{q} + q_V. \tag{0.19}$$

For a function u(x,y,z,t) of three spatial variables (x,y,z) and time t, the heat conduction equation is

$$\frac{\partial u}{\partial t} = \alpha \left(\frac{\partial^2 u}{\partial x^2} + \frac{\partial^2 u}{\partial y^2} + \frac{\partial^2 u}{\partial z^2} \right) \tag{0.20}$$

For any coordinate system: $$\frac{\partial u}{\partial t} - \alpha \nabla^2 u = 0, \tag{0.21}$$

were α - is a positive constant, and a is the Laplace operator.

If we take into account the rate of heat propagation (i.e., consider it in dynamics), then an additional term appears in the expression for the Fourier heat flux density:

$$\overline{q} = -\lambda grad(T) - T_r \frac{\partial \overline{q}}{\partial t} \tag{0.22}$$

The main disadvantage of this approach to analyzing the temperature field is the uncertainty in choosing the thermal conductivity coefficients of the components of an electric machine and the values of heat transfer coefficients.

In order to clarify these parameters, the calculation is based on the application of the laws of thermal conductivity, and the values of the coefficients of thermal conductivity and heat transfer are determined experimentally on model installations. At the same time, of course, it is necessary to operate with the concepts of average values of heat conduction and heat transfer coefficients related to the machine as a whole, or to large structural components [11].

The basic law of heat conduction defines the amount of heat that passes through a surface dF in time depending on the temperature gradient and material properties. If $\frac{\partial \bar{q}}{\partial t} = 0$, then expression (2.22) will have the form

$$\bar{q} = -\lambda grad(T) \tag{0.23}$$

were λ – thermal conductivity coefficient (thermal characteristic of the material), [Wt/(m·K)].

The temperature gradient is a vector directed along the normal to the isothermal surface in the direction of temperature growth and numerically equal to the partial derivative of the temperature in this direction. The positive direction of the gradient is the direction of temperature increase.

Consider the nature of the temperature change with wall thickness and the heat flow through the wall. An infinitely large flat wall with a thickness of thermal conductivity transfers heat at constant temperatures at the boundary T1 and T2 (boundary conditions).

$$\frac{\partial T}{\partial t} = a\left(\frac{\partial^2 T}{\partial x^2} + \frac{\partial^2 T}{\partial y^2} + \frac{\partial^2 T}{\partial z^2}\right). \tag{0.24}$$

Under the conditions under consideration, heat can only propagate along the x-axis, and the temperature field will be one-dimensional:

$$\frac{\partial^2 T}{\partial^2 x} = 0. \tag{0.25}$$

After integrating expression (2.24) and substituting T1 and T2, we obtain the equation of the temperature field:

$$T = \frac{T_1 - T_2}{\delta} x + T_1, \tag{0.26}$$

$\delta = x$ - wall thickness on the temperature side T2.

Heat flux density through a flat wall:

$$q = -\lambda \frac{dT}{dx} = \frac{\lambda (T_1 - T_2)}{\delta}, \tag{0.27}$$

$\frac{\lambda}{\delta} = R$ – thermal resistance of a flat wall.

The further solution is to consider the thermal substitution scheme, which uses the analogy with Ohm's law for an electrical circuit. Thermal resistances are extracted from simple geometric shapes into which the entire electrical volume can be divided, the model of the electric motor.

Thermal calculation of an electric machine due to the complexity of the heat flow pattern is performed under a number of assumptions. When choosing the assumptions, it is taken into account that the calculation methodology, firstly, must meet practical goals in terms of the accuracy of the results and, secondly, must require a disproportionately large amount of calculation work. In addition, the degree of accuracy of even the most mathematically precise calculation is no higher than that achieved in determining the coefficients included in the calculation formulas.

When considering the physical process of heat dissipation from the surface and the effect of ventilation on the heat transfer coefficient, it turned out that instead of the true, real dependencies determined from experience with schematic samples of machine parts, simplified dependencies are usually taken, which have an accuracy of about 5% relative to the true values of certain physical dependencies.

2.6 Estimation of the influence of temperature dependence of parameters on the properties of a thermodynamic model of an electric machine

Effect of temperature on heat capacity.

Figure 2.3 shows graphs of the specific heat capacity of copper, aluminum, and iron in J/(kg-K) versus temperature (the points represent experimental data [10]). This figure shows that the experimental points are very well approximated by the equation of the form

$$C_{пит} = \alpha_c \theta^2 + b_c \theta + c_c$$

α_c, b_c та c_c – constant coefficients, the values of which are shown in the table 2.1.

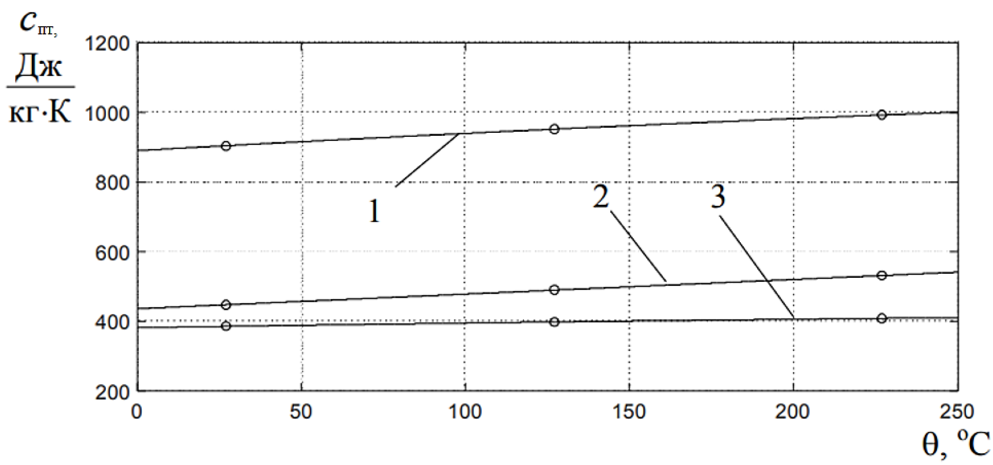

Рисунок 2.3 – Graphs of the specific heat capacity of metals versus temperature: 1 - aluminum; 2 - iron; 3 - copper

Таблиця 2.1 – Coefficients of dependence of the specific heat capacity of metals on temperature

Metal	α_c, J/(kg ×К^2)	b_c, J/(kg×К^2)	c_c, J/(kg ×К^2)
Copper	$-1{,}200 \cdot 10^{-4}$	0,1455	381,2
Aluminum	$-3{,}525 \cdot 10^{-4}$	0,5303	889,6
Iron	0	0,4200	435,7

Copper	1,027	1,035	1,041
Aluminum	1,043	1,056	1,066
Iron	1,057...1,064	1,075...1,084	1,089...1,101

From the data in Table 2.2, it follows that taking the heat capacity of the machine elements equal to the average value for the actual temperature range, we ensure an error value not exceeding 5%, which can be considered acceptable in most cases. However, in a multi-mass fuel cell, the temperature range of different nodes differs significantly, which creates some uncertainty when choosing the above average value.

Effect of temperature on thermal conductivity

Metals.

Copper. [10, 11] provide data on the thermal conductivity of copper, according to which, with an increase in temperature from 300 to 400 oC, the thermal conductivity of copper decreases by only 2.0% (from 401 to 393 W/(m-K)), which allows us to consider it constant in the temperature range relevant for modeling electrical machines.

Aluminum. The data on the thermal conductivity of aluminum given in [10, 11] show that with an increase in temperature from 300 to 400 oC, the thermal conductivity of aluminum decreases by only 1.27% (from 240 to 237 W/(m-K)), which also allows us to consider it constant in the temperature range relevant for modeling electrical machines.Cast iron. The thermal conductivity of cast iron depends on its chemical composition, but, according to [11], for ordinary cast iron, when the temperature changes from 0 to 100 °C, it decreases slightly, within 3.6...5.1%.

Steel. The decrease in the thermal conductivity of electrical steel with increasing temperature is much stronger than that of copper, aluminum, and cast iron. It can decrease by 20...25% with an increase in temperature by 40°C. However, accounting for this phenomenon when building a thermodynamic model is complicated by a number of factors. For example, the thermal conductivity of a steel package can vary significantly along and across the rolled products: in the transverse direction of the charge packages, it is significantly lower than along the sheet and depends on the pressure of the sheet pressing [10]. Thermal conductivity also depends on the steel grade [10]. For example, the thermal conductivity of steel decreases significantly with an increase in the percentage of silicon [12].

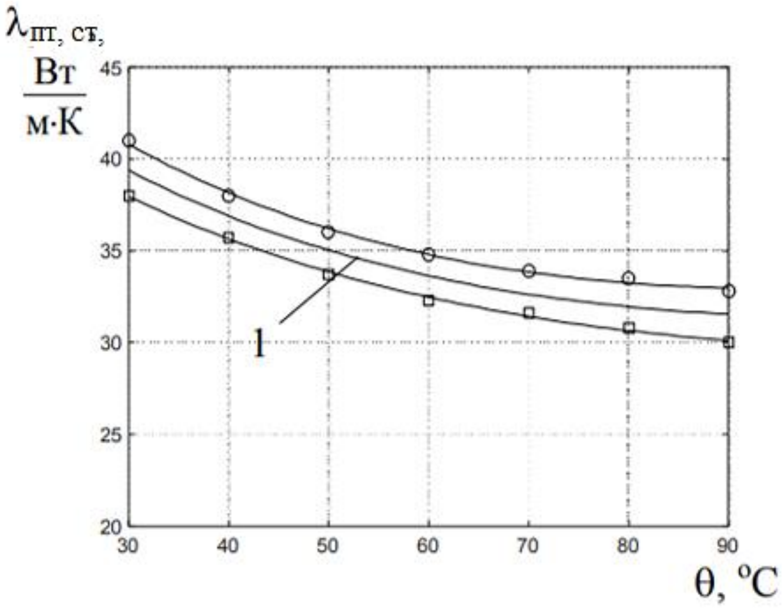

Figure 2.4 - Dependence of thermal conductivity of steel in 2013 on temperature (marked: ○ - along the rolled products; □ - across the rolled products; 1 - averaged values)

The dependence of the specific thermal conductivity of steel on temperature can be approximated by the following expression:

$$\lambda_{п.в} = (\alpha_k \theta^2 + b_k \theta + c_k)^{-1}$$

where the constant coefficients, for example, for the averaged values of the specific thermal conductivity of steel in 2013 are equal to: $\alpha_k = -1{,}321 \cdot 10^{-6}$; b_k $=2{,}634 \cdot 10^{-4}$; $c_k = 1{,}869 \cdot 10^{-2}$.

Air. The thermal conductivity of air increases almost linearly with increasing temperature. Figure 2.5 shows the graphs of the dependence of the thermal conductivity of air on temperature (the points show the experimental data from [10]).

Figure 2.5 shows that the experimental points are very well approximated (standard deviation 0.07%) by a linear function: $\lambda_{п,пов} = 7.078 \cdot 10^{-5}\theta + 0.0237$.

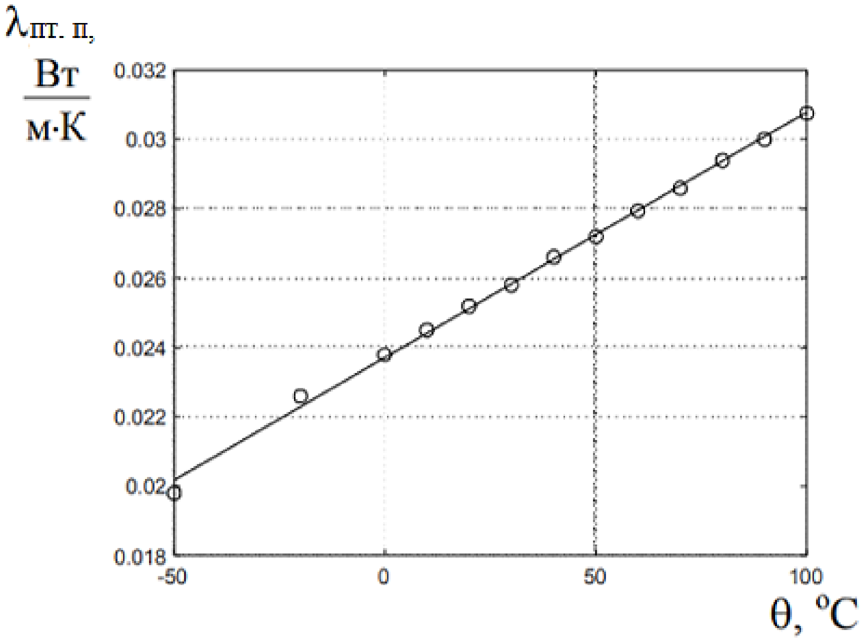

Figure 2.5 - Dependence of air thermal conductivity on temperature

Figure 2.5 shows that the thermal conductivity of air changes very significantly in the temperature range relevant for modeling the TDM processes. The thermal conductivity of air is included as a factor in the expression for calculating heat transfer from the closed AP body, so the temperature dependence of this thermal conductivity can have a certain effect on the steady-state temperature of engine components. For blower motors, the influence of this factor is less significant, since the heat transfer coefficient from the casing is determined by the blowing efficiency. For closed electric machines that are not blown, the temperature dependence of the heat transfer coefficient from the housing may play a more significant role, since the analysis of the graphs of this dependence given in [7, 8] shows that when the housing temperature increases by 60 °C, the change in the heat transfer coefficient can be within this temperature range exceed 10% of the average value. This means that the effect of increasing heat transfer with increasing temperature must be taken into account when building the model.

It should be noted that the heat flows from the motor winding to the cooling air may include air spaces (e.g., air in the inner casing of a closed motor). However, the resulting thermal conductivities through such paths will be influenced by the thermal conductivities through the metal, which depend on temperature in different directions from the air, thus partially compensating for the temperature effect.

Thus, the situation with regard to the temperature-dependent thermal conductivity of an electric machine model is very complex. The thermal conductivities of metals and air change in different directions with temperature. For example, the thermal conductivity of metal structural elements tends to decrease with increasing temperature, but to varying degrees depending on the material and its processing, and the thermal conductivity of air, including heat transfer from the surface to the environment, increases with increasing temperature. This circumstance can be taken into account when building a sufficiently detailed model for further numerical solution, but it cannot be “directly” taken into account in the analytical study of the system of equations of this mathematical model, since it leads to the appearance of a nonlinearity of the mathematical description of the TDM. It is also difficult to take into account the temperature change of parameters when constructing a model from a small number of elements, where elements with different

2.7 Influence of temperature dependence of heat capacitances and thermal conductivities on the calculation results

Influence of temperature changes in thermal conductivities on the steady-state temperature of the fuel assembly. Figure 2.6 shows graphs of the calculation error of the temperature excess of the thermodynamic model components as a function of the relative value of the engine torque where, is the temperature excess of the fuel assembly components, taking into account the temperature change in thermal conductivities (the ambient temperature was assumed to be 20 ºC); τ_{0i} – Exceeding the temperature of the TDM elements, without taking into account the temperature change in thermal conductivities (according to the average values of the temperature range), - node number of the thermodynamic model. The temperature change in the winding resistance was taken into account in both cases, the graphs were plotted for an ambient temperature of 20 °C was taken into account in both cases, the graphs were plotted for an ambient temperature 20 °C.

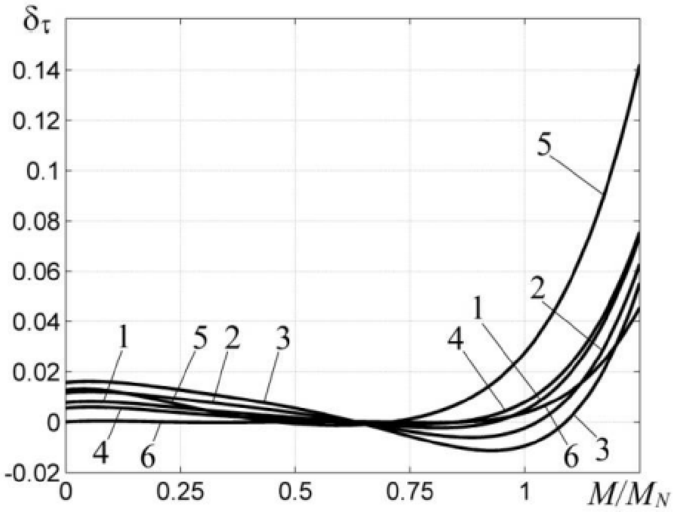

Figure 2.6 - Calculation errors of the temperature exceedance of the thermodynamic model components in steady-state mode (1 - winding lobes; 2 - winding groove; 3 - stator; 4 - internal air; 5 - rotor; 6 - bed).

Figure 2.6 shows that in the temperature range that does not exceed the values corresponding to the rated operating mode, the calculation error is not significant and does not exceed 3%. From this, it can be concluded that in a thermodynamic model focused on operating modes in which temperature deviations from the average values are not large and the average values do not exceed those corresponding to the nominal operating mode (), it makes no sense to take into account the temperature change in thermal conductivity. At the same time, it should be borne in mind that ignoring the temperature dependence of thermal conductivity can lead to serious calculation errors at temperatures exceeding . Thus, when calculating the excess temperature of the frontal parts of the stator winding of the 4A100L4 motor at a load of 140% of the rated torque, taking into account the temperature change in thermal conductivity, we obtain 195.8°C, and without taking it into account 240.7°C. Taking into account the exponential nature of the dependence of the winding insulation thermal aging rate on its temperature [12], such a discrepancy should be considered unacceptable for the task of assessing the thermal state of the motor.

b) The effect of temperature changes in heat capacities and thermal conductivities on the TDM time constants. Working with different loads, the components of the TDM have different temperatures. This affects the heat capacitances of the components and the thermal conductivities between them, which leads to changes in the time constants with load changes. Figure 2.7 shows the graphs of the ratio of time constants T0j/Tj of the six-mass thermodynamic model of the 4A100L4 engine as a function of the relative value of the engine torque, Here, T0j is the time constant without taking into account the temperature dependence of heat capacities and thermal conductivities; Tj is the time constant with the temperature dependence of these parameters; j is the number of time constants in ascending order of their value.

When calculating the time constants, we approximated the dependence of thermal conductivities on temperature using the formulas and took into account the composition of various materials in the thermal conductivity links.

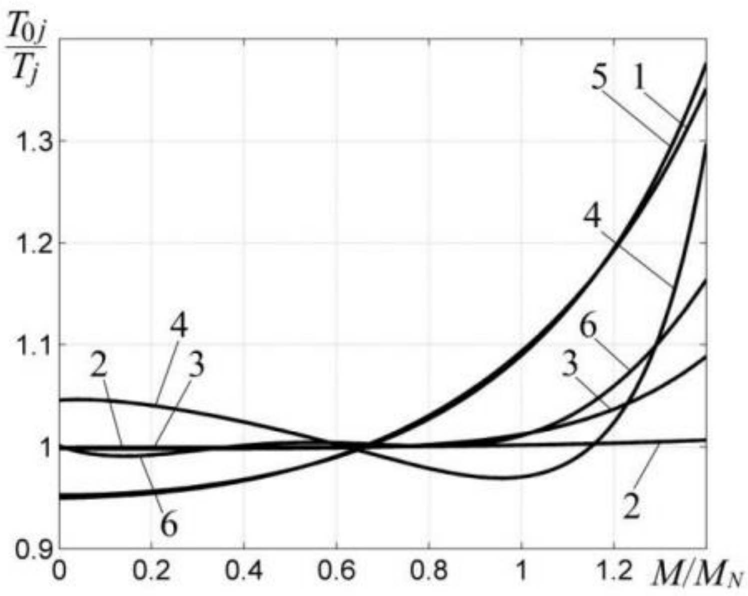

Figure 2.7 - Dependence of the relative values of the time constants of the TDM on the load on the shaft (the numbers indicate the numbers of time constants in ascending order of their value)

The analysis of the graphs in Figure 2.7 allows us to note that in the temperature range not exceeding the value of , the error in calculating the time constants is not large and only for the first and fifth constants approaches 10%, while the first constant is associated with the heat capacity of the internal air, which is less than 1 s and does not significantly affect the winding temperature dynamics. When calculating processes in which the temperatures of the model nodes significantly exceed the value of , it is necessary to take into account the effect of temperature on the time constants due to the temperature dependence of heat capacities and thermal conductivities, since the difference between Tj and T0j is significant for the three largest time constants. Two of these constants (the fourth and fifth) have values that are within the formal limit of the duration of the repeatedly short-term operation mode, so the components of the solution containing these constants may change at intervals of appropriate duration, affecting the accuracy of the modeling results.

2.8 Development of the geometry of the motor model

To calculate the electrical and temperature characteristics of the AC motor, an asynchronous squirrel-cage motor was selected. Its basic passport data is given below.[14]

- Frequency: 50 Hz
- Rated power: 2.2 kW
- Rated voltage: 220/380 V
- Rated current: 4,56 A
- Number of poles: 4
- Room temperature: from -20 ^{o}C до +40 ^{o}C
- Efficiency at rated load: 87 %
- Power factor, at rated load: 0,8
- Rated load speed: 1435 r/V
- Operating temperature range: from -20 ^{o}C до +40 ^{o}C
- To develop a motor model in the FluxMotor program, you need to draw its geometry. The main dimensions of the stator and rotor are given below
- Main characteristics of the stator:
- Axial length of the core: 120 mm
- Diameters: outer (160 mm) and inner (100 mm)
- Number of stator teeth: 36

Air gap thickness: 0.3 mm

- *Main characteristics of the rotor:*
- Axial length of the core: 120 mm
- Diameters: outer (99.4 mm), inner (35 mm)
- Number of rotor teeth: 28

Number of rotor teeth:

- Conductor diameter: 0.75 mm

- Winding type: concentric, combined pitch and single-layer Winding steps: 1:8:10 / 1:8 Number of turns: 36
- Connection: star,
- Stator phase resistance: 1.91 ohms, at 20ºC

The software must mathematically recognize the entire structure to be able to perform the entire calculation process. To do this, a mesh must be created. This allows the geometry of the motor to be discretized into small elements, at intermediate nodal points, approximated by computational methods. Using definitions such as deflection type, relaxation type, and point type, the software automatically adjusts all sets of elements according to the size and complexity of the faces, The geometry of the engine model and the partitioning mesh in two dimensions is shown in Figure 2.8.

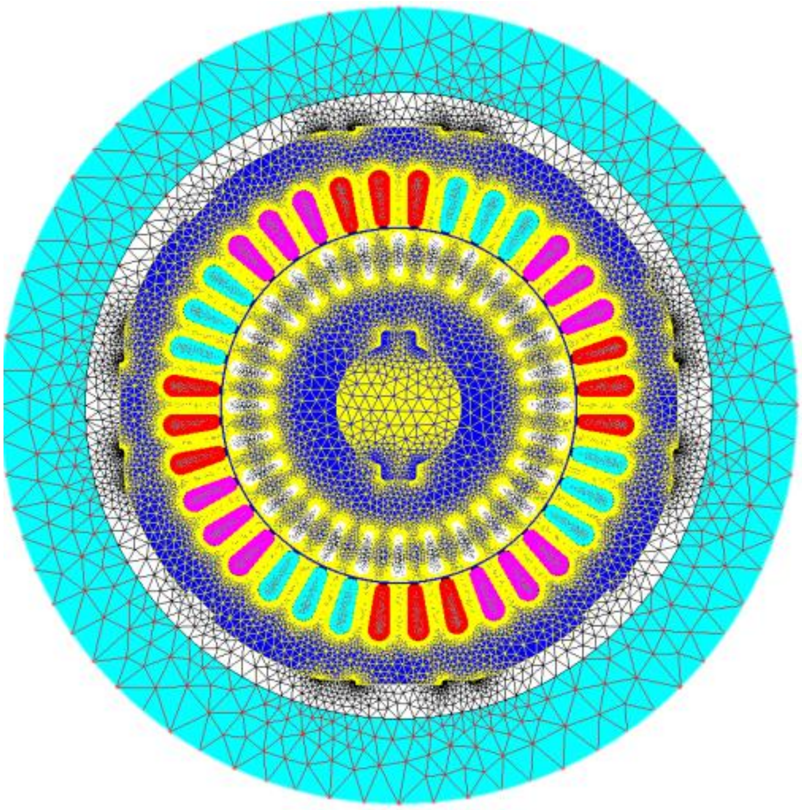

Figure 2.8 Finite element mesh of the electric motor model

The mesh is denser in the air gap area due to the need for greater accuracy in the calculations.

For electromagnetic modeling in the FluxMotor program, it is necessary to assign the appropriate material to each element of the model geometry. For example. To do this, it is necessary to enter their magnetic and electrical properties, as well as their density. In the motor model, the coils are made of copper, the stator is made of electrical steel, and the rotor rods are made of aluminum. The electrical and magnetic parameters of the materials are shown in Table 2.3.

The modeling will assume that the moving part of the geometry is the rotor and the air gap. All other elements of the model are fixed. This condition will allow the program to correctly model the rotational motion of the model structure.

Table 2.3 Electrical and magnetic parameters of model materials

Copper	
Relative magnetic permeability	1
Resistivity	$1{,}72\cdot10^{-8}$ Ω·m
Density	8940, кг/m^3
Aluminum	
Relative magnetic permeability	1
Resistivity	$2{,}7\cdot10^{-8}$ Ω·m
Density	2698, кг/m^3
Electrical steel	
Initial relative permeability	11368,21
Saturation magnetization	1,97, T
Resistivity	$4{,}8\cdot10^{-7}$ Ω·m
Density	7650, кг/m^3

The following assumptions were made in the model construction:

1. The field in the engine core is plane-parallel, the field pattern in any cross-section of the machine is the same.

2. The field of the windings' frontal parts is not considered, the influence of edge effects is not taken into account.

3. The currents in the motor winding vary in time according to a harmonic law. The influence of time harmonics is not taken into account.

2.9 Conclusions to the section

1. It has been shown that in electric motors, the thermal and electromagnetic fields are interconnected and directly affect their design. Among the existing modelling methods, a numerical method for calculating the field based on the finite element method was chosen.

2. The mathematical models for calculating electromagnetic and thermal fields are presented, which allow determining losses in motors and temperatures of its elements, both in the stationary and transient processes.

3. The analysis shows the importance of taking into account the temperature change in winding resistance when constructing thermodynamic models of electric machines. It is shown that the temperature change of the windings will be insignificant within the cycle, but the average temperature level of the model nodes will significantly depend on the fact of taking into account the temperature change of the resistances. The temperature dependence of the thermal conductivities and heat capacities of copper and aluminium can be ignored in most cases. Ignoring the temperature dependence of the thermal conductivities of air and steel, as well as the heat capacity of iron-containing engine components, can lead to significant calculation errors.

4. The geometry of the model of an induction motor with a squirrel-cage rotor was developed in the FluxMotor software based on its passport data. A finite element mesh was constructed and electrical and magnetic parameters of materials were assigned to the model elements

3 CALCULATION SECTION

3.1 Preliminary calculation of motor parameters

Since it is of interest to find the electrical and temperature characteristics of the motor under nominal conditions, it is necessary to first find the slip value. Knowing that this is a four-pole machine and its rated speed is 1450 rpm at 50 Hz, equations (3.1) and (3.2) were used to calculate the rated slip. The result was approximately 0.0433, so this value will be used from now on.

$$n_s = \frac{60 \cdot f}{p} \tag{3.1}$$

$$s_n = \frac{n_s - n_n}{n_s} \tag{3.2}$$

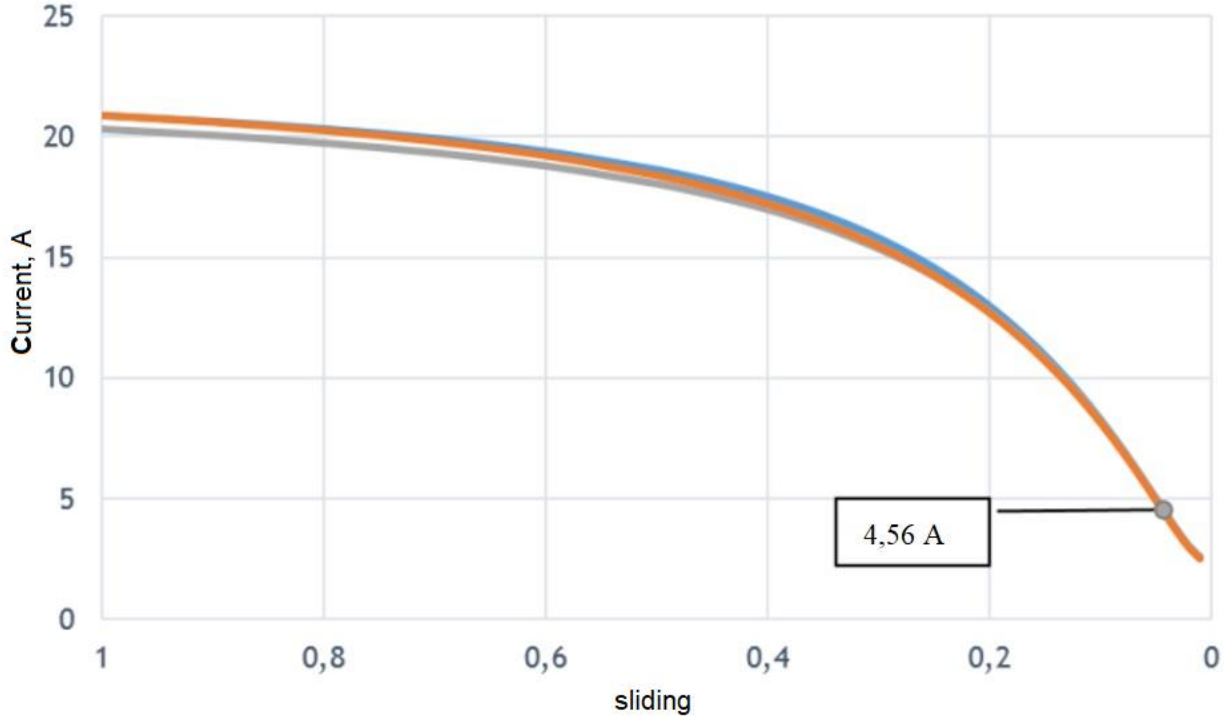

Figure 3.1 - Input current versus sliding

In Figure 3.1, the three-phase currents are presented as a function of slip, where you can see that each phase starts with a high current value and drops while the slip decreases. This high current value is completely normal because during motor start-up, current values can reach approximately eight times the rated current value. They should be equal, but in the starting period they are not. This is due to the random initial relative position between the rotor and stator. While the number of stator teeth is 36 and the number of poles is 4, the number of rotor rods is 28, which is not divisible by 3. This means that the rotor resistance per phase is different for the three phases. While the motor is rotating, all current values tend to reach the same value. When the rated condition is reached (at rated slip), you can see that the current value is equal to the value on the motor nameplate (4.56 A).

Fig. 3.2 shows the curve of the mechanical torque as a function of slip, where the rated operating point is indicated.

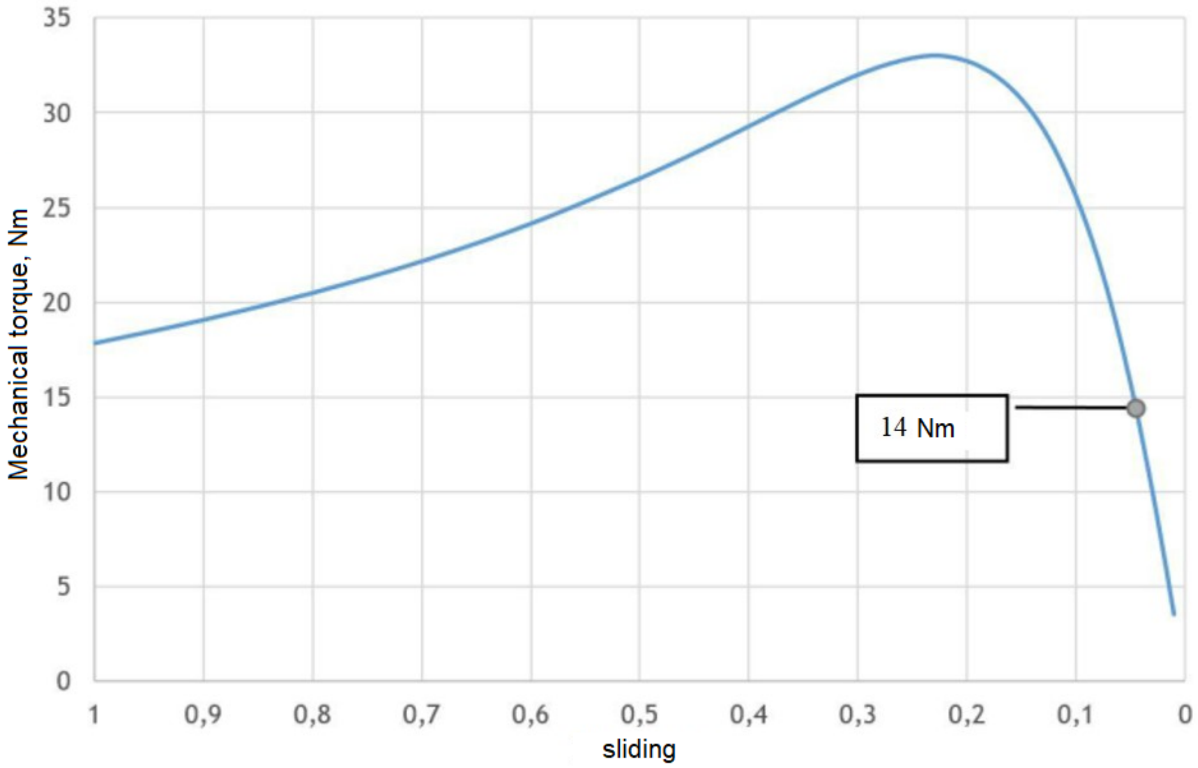

Figure 3.2 - Dependence of mechanical torque on sliding

To make sure that the simulation results are close to the expected results, it is necessary to calculate the torque at the rated condition. For a nominal motor speed of 1435 rpm, the mechanical power is 2.2 kW The calculated value was 14.64 Nm.

The change in mechanical power as a function of slip is shown in Figure 3.3, along with the nominal condition point.

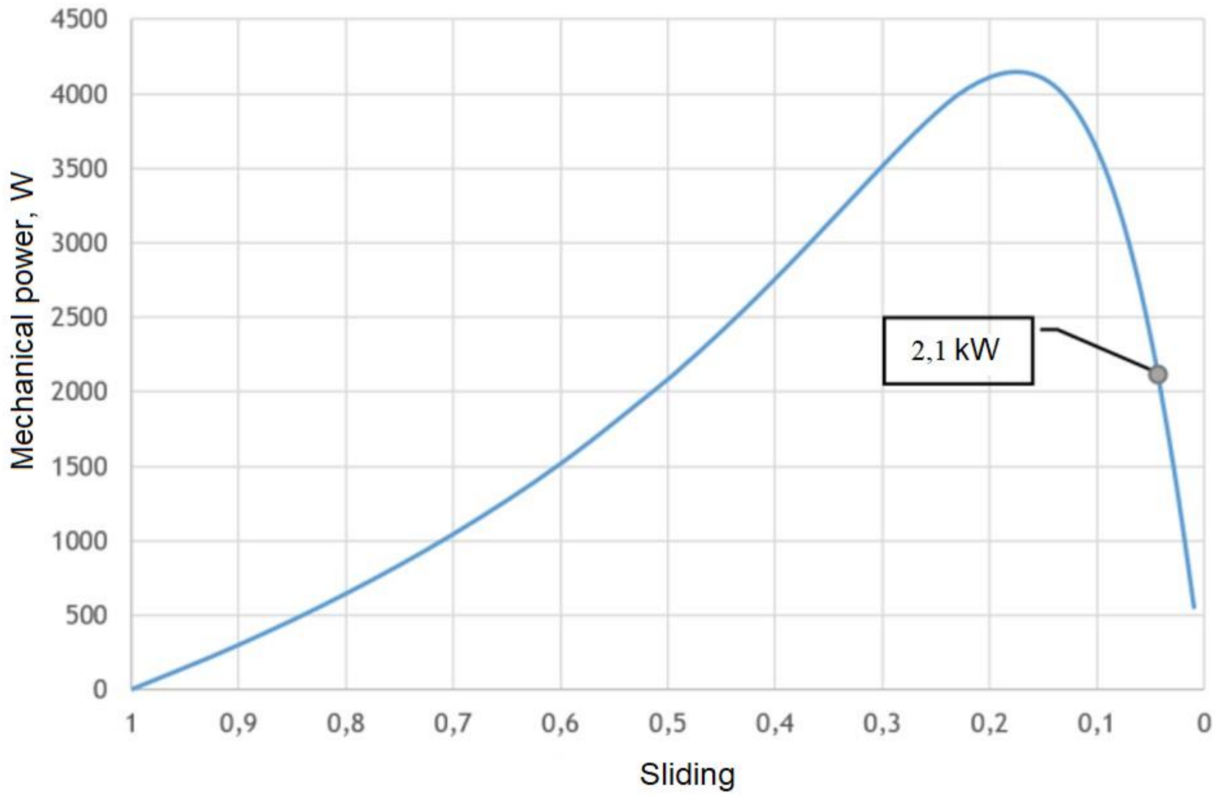

Figure 3.3 - Dependence of mechanical power on sliding.

3.2 Calculation of losses

To calculate the temperature field, it is necessary to know the losses in the motor. After analysing the results and determining the slip, it is necessary to focus on the nominal slip point to calculate the losses in the conductors and the magnetisation losses.

The stator coil losses are 158.21 W, which is the sum of the winding losses of the three windings of the induction motor. The rotor losses are 55.43 W.

The software calculates stator and rotor losses using the Bertotti method. To calculate them, the dependence of the specific losses on the magnetic flux is used. Figure 3.4 shows this characteristic for rotor and stator steel.

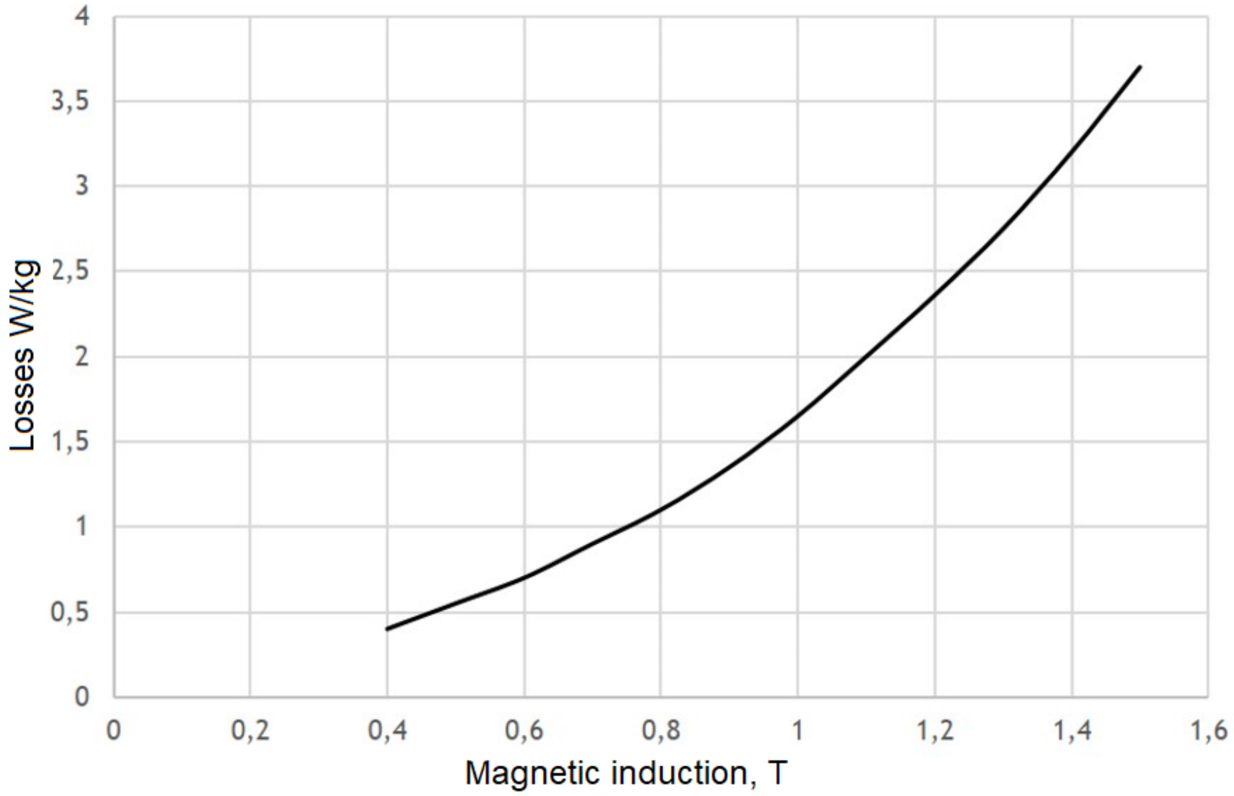

Figure 3.4 - Dependence of steel losses on magnetic flux

Losses in magnetic materials are defined as the sum of two types of losses: hysteresis losses and eddy current losses. The results of the calculation of losses in the steel are shown in Table 3.1.

Table 3.1 - Losses in the stator and rotor

Type of losses	Stator, W	Rotor, W
Hysteresis	19,184	0,008
Eddy currents	4,63	0,000
Total losses	23,814	0,008

3.3 Temperature calculation of the motor

This section presents the thermal results obtained from a two-dimensional simulation. This thermal simulation lasted for 10,000 seconds (approximately 2 hours and 47 minutes) and the initial temperature was set to 21°C. In order to better understand the thermal behaviour throughout the process, some intermediate steps are presented. Figure 3.5 shows the motor temperatures from the initial step (0 seconds) to the last step (10000 seconds). It can be seen that the rotor and stator temperatures are the same at the beginning of the simulation; however, this starts to change somewhere between 1000 and 2000 seconds. In other words, between these values, the rotor starts to heat up more than the stator.

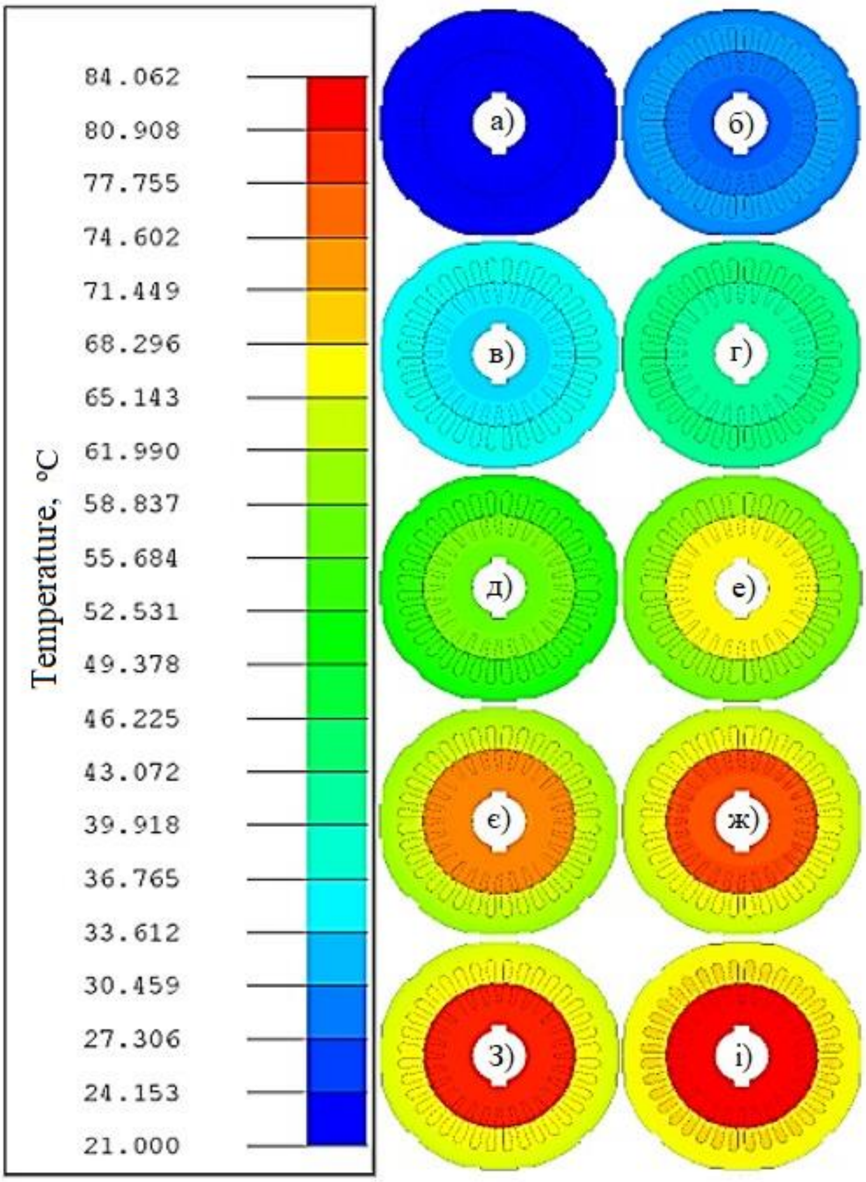

Figure 3.5 - Thermal behaviour of the engine at a point in time: a) 0 s; b) 300 s; c) 600 s; d) 1000 s; e) 2000 s; e) 3000 s; f) 4000 s; g) 5000 s; h) 6000 s; i) 10000 s

Below are more specific results on the thermal behaviour of the engine for some of the simulation stages.

Figure 3.6 shows that after 600 seconds (10 minutes), the motor is still in the process of initial heating, although the temperature has already started to rise. You can now see that the rotor and stator temperatures are quite different. The lowest temperatures are inside the rotor, near the shaft, and the highest temperatures are in the stator coils, with a difference of about 3.5°C. The lowest stator temperatures are observed in the outer part of the stator due to air convection.

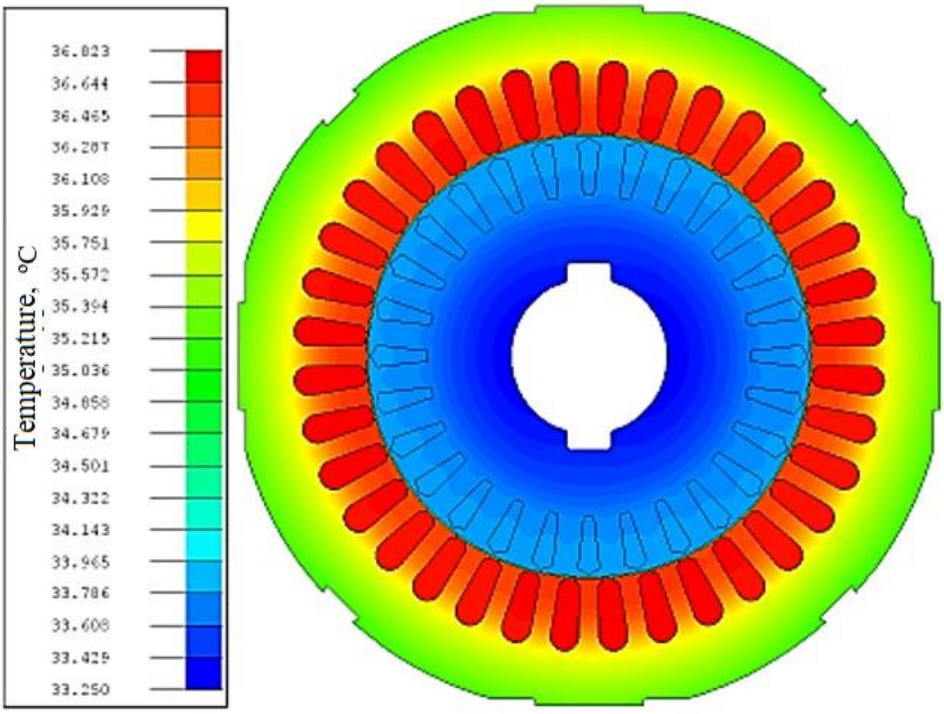

Figure 3.6 - Thermal behaviour of the motor after 600 s.

Figure 3.7 shows that by the time of 1200 seconds (20 minutes), the motor has already doubled the initial temperature distribution. Although the stator coils have the highest temperatures, the difference between them and the rotor rods is decreasing. At this point, these temperatures are already about 0.5°C different. It can also be seen that the temperature difference between the lowest and highest points of the stator has increased.

After 2000 seconds (33 minutes and 20 seconds), Figure 3.8 shows that the rotor temperature has already exceeded the stator coil temperature due to the influence of the rotor rods.

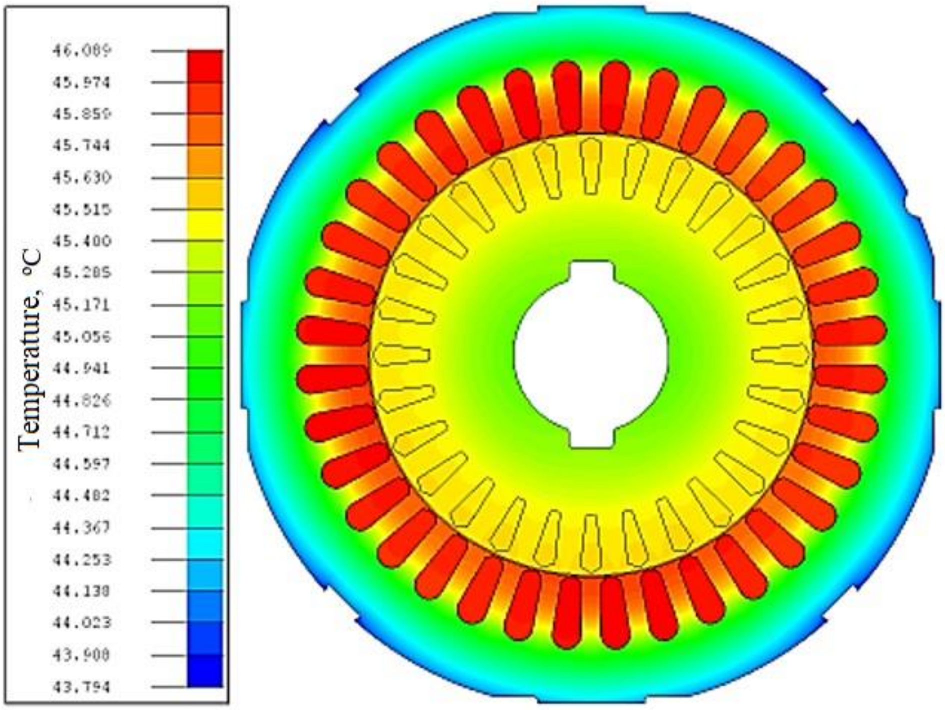

Figure 3.7 - Thermal behaviour of the motor after 1200 s.

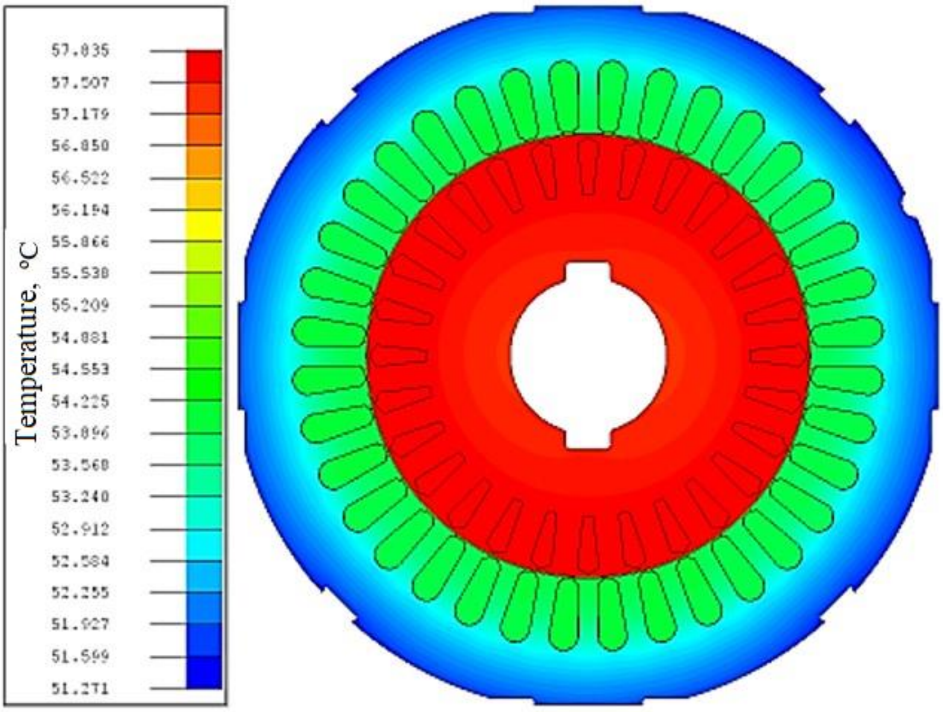

Figure 3.8 - Thermal behaviour of the motor after 2000 seconds.

After 6000 seconds (1 hour and 40 minutes), Figure 3.9 shows that the difference between the rotor and stator temperatures continues to grow, at this point being approximately 12°C. At this point, the motor temperature has almost stabilised.

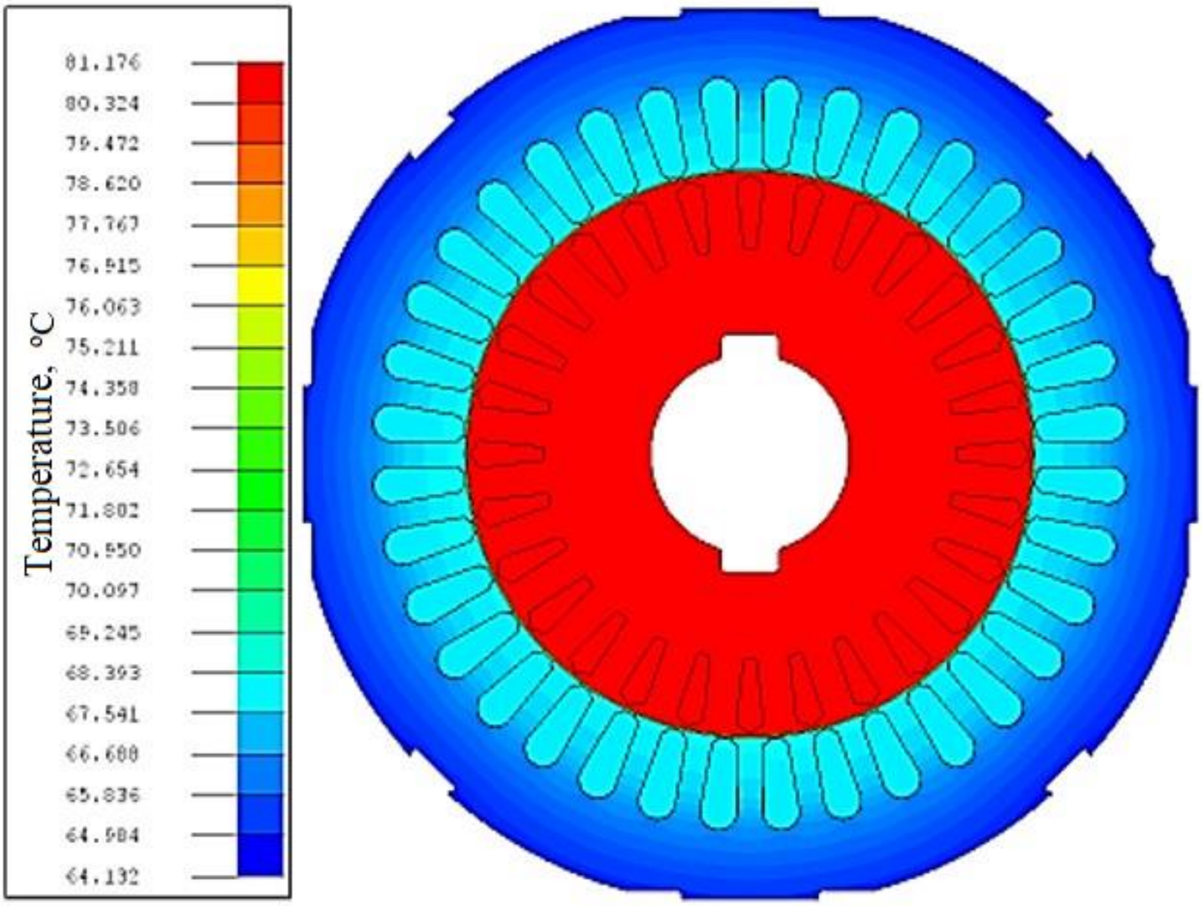

Figure 3.9 - Thermal behaviour of the motor after 6000 s.

Figure 3.9 shows that the thermal behaviour of the engine has not changed much since the previous step (6000 seconds).

Figure 3.10 shows the temperature field after 10000 seconds of simulation (2 hours, 46 minutes and 40 seconds), the motor temperature has already stabilised, After reaching a stable operating point, it can be stated that the temperature difference between the rotor and stator is about 13ºC and the difference between the coldest and hottest points of the stator is about 5.5ºC.

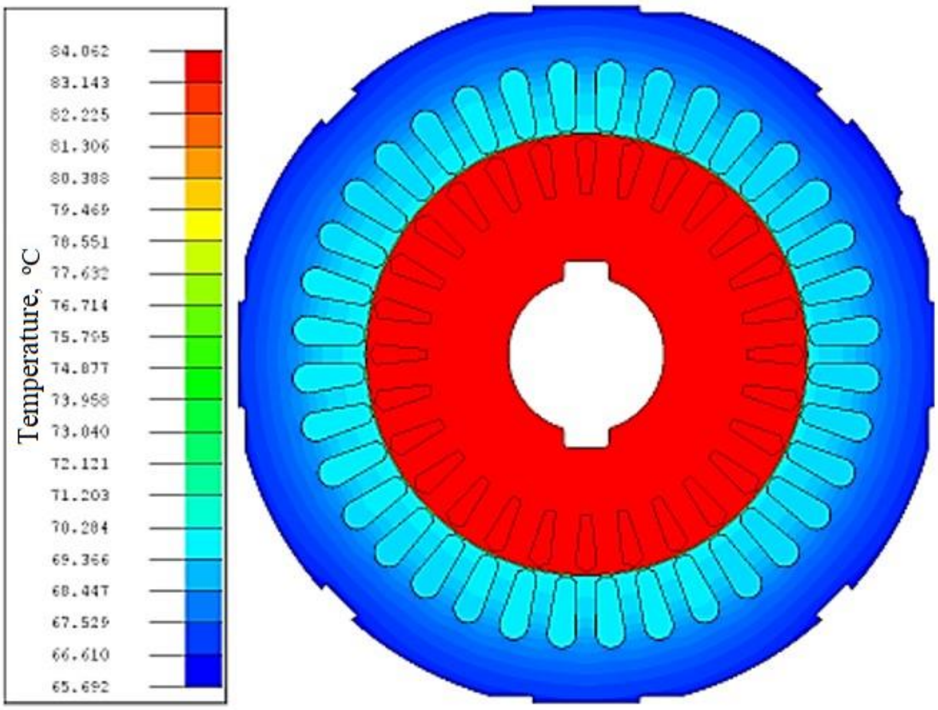

Figure 3.10 - Thermal behaviour of the engine after 10000 s.

3.4 Modelling motor operation in loaded mode

An important step is to simulate the behaviour of the induction motor with a load connected. In this simulation, the motor will start at zero speed. The initial value of inertia will be 0.00897 kg-m2. The value of the torque will change during the simulation. First, the motor will start in idle mode (T = 0 N-m) and then increase to the rated operating load (T = 14 N-m). This time dependence is shown in Figure 3.11.

Inrush currents can reach values up to about 8 times their nominal value, so the initial values are expected (Figure 3.12).

After that, the current values decrease as the motor is running at no-load (T = 0 N-m). In this state, the current values are around 2.85 A, but this is the peak value.

The effective value can be calculated by dividing it by √2. The rms value of the no-load current is therefore about 2.02 A.

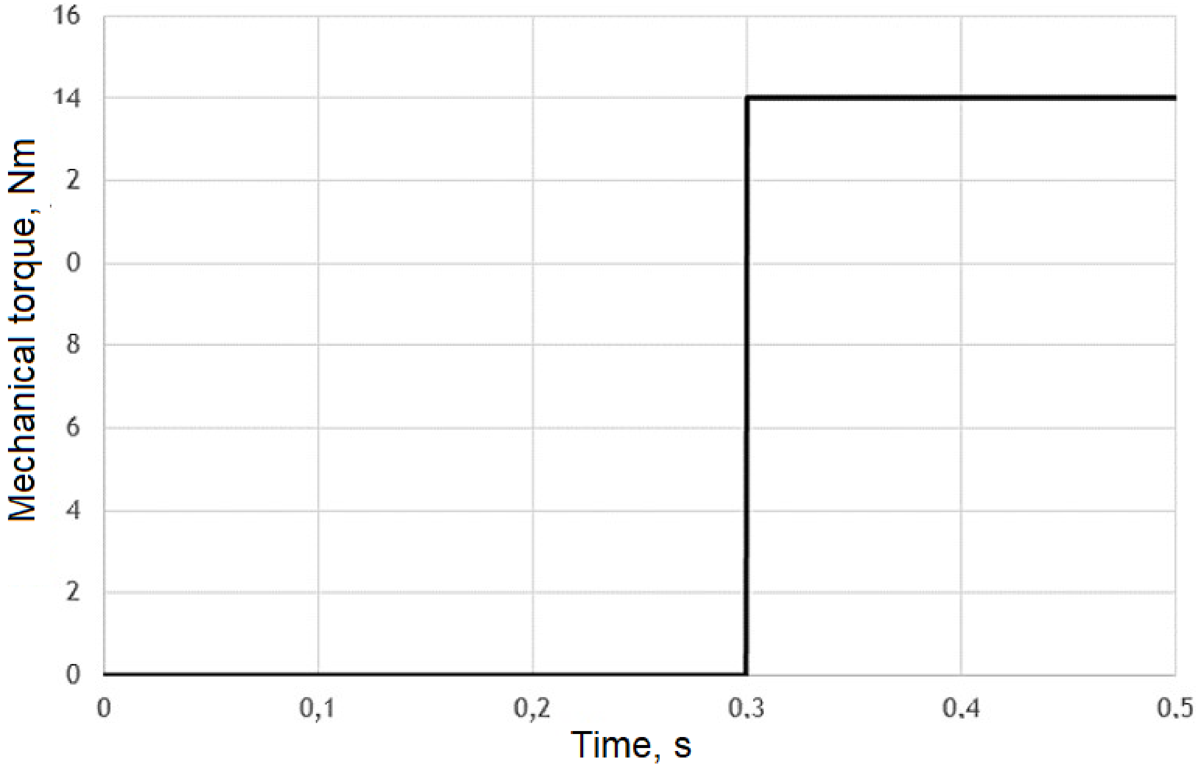

Figure 3.11 - Time dependence of the mechanical torque of the motor

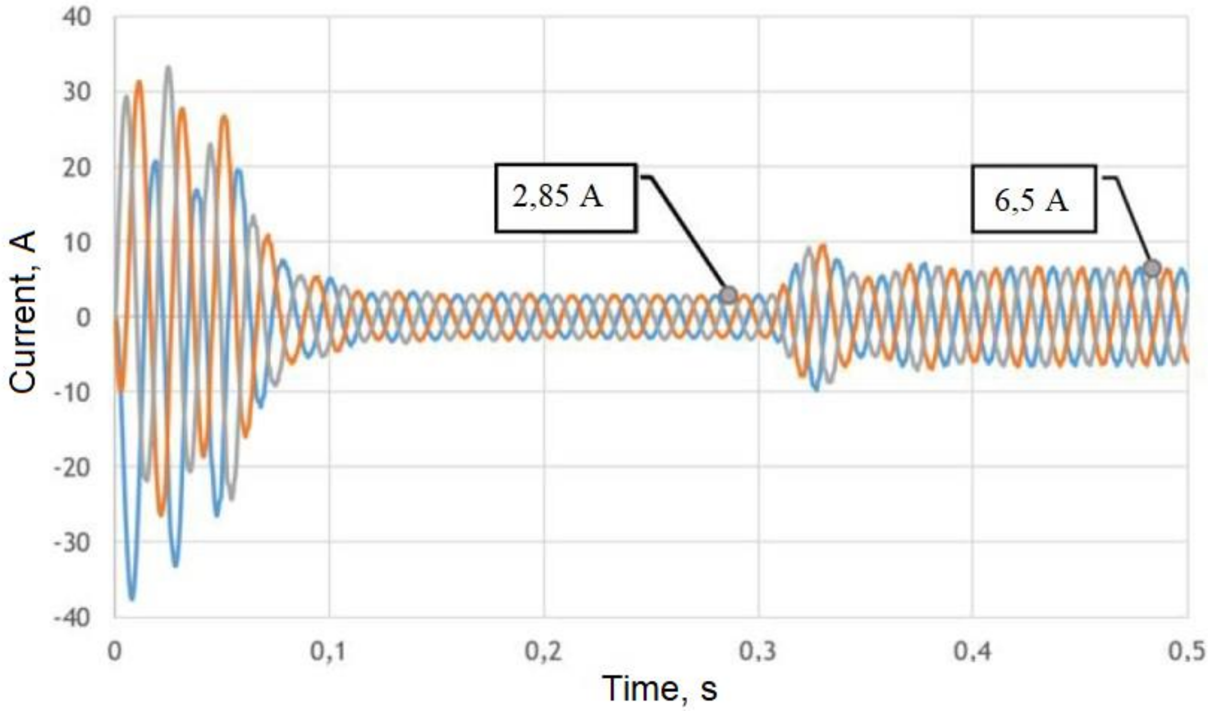

Figure 3.12 -- Motor operating current

At the 0.3 second time point, the mechanical torque increases and so does the current, reaching the rated current. The value of the rated current obtained in the simulation is $6.5\sqrt{2} \approx 4.6$ A.

As can be seen in Figure 3.13, the engine starts at zero speed, and then the speed starts to increase until it stabilises at idle, at a speed of approximately 1499 rpm.

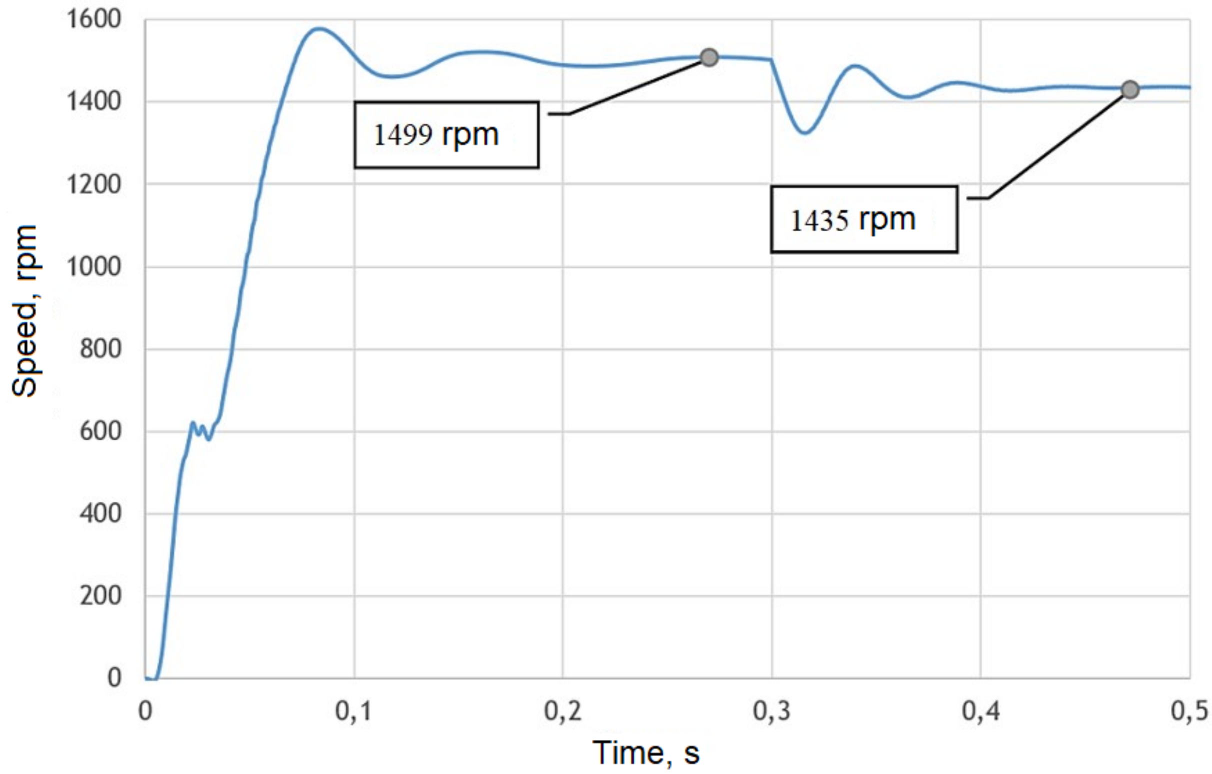

Figure 3.13 Graph of the engine speed dependence

Starting from 0.3 seconds, the motor is operating under rated load conditions. This means that the mechanical torque has increased, so the speed drops and stabilises at 1435 rpm. This value is equal to the motor's nameplate value.

In the previous paragraph, the optimal slip value was determined to be close to 1, so the initial mechanical torque reaches very high values. After that, in Fig. 3.14, you can see that this value drops to a very low value close to 0 Nm. At this point, the motor is running without load. After 0.3 seconds, the motor starts to run under rated load conditions, and the expected mechanical torque value of 14 Nm can be seen.

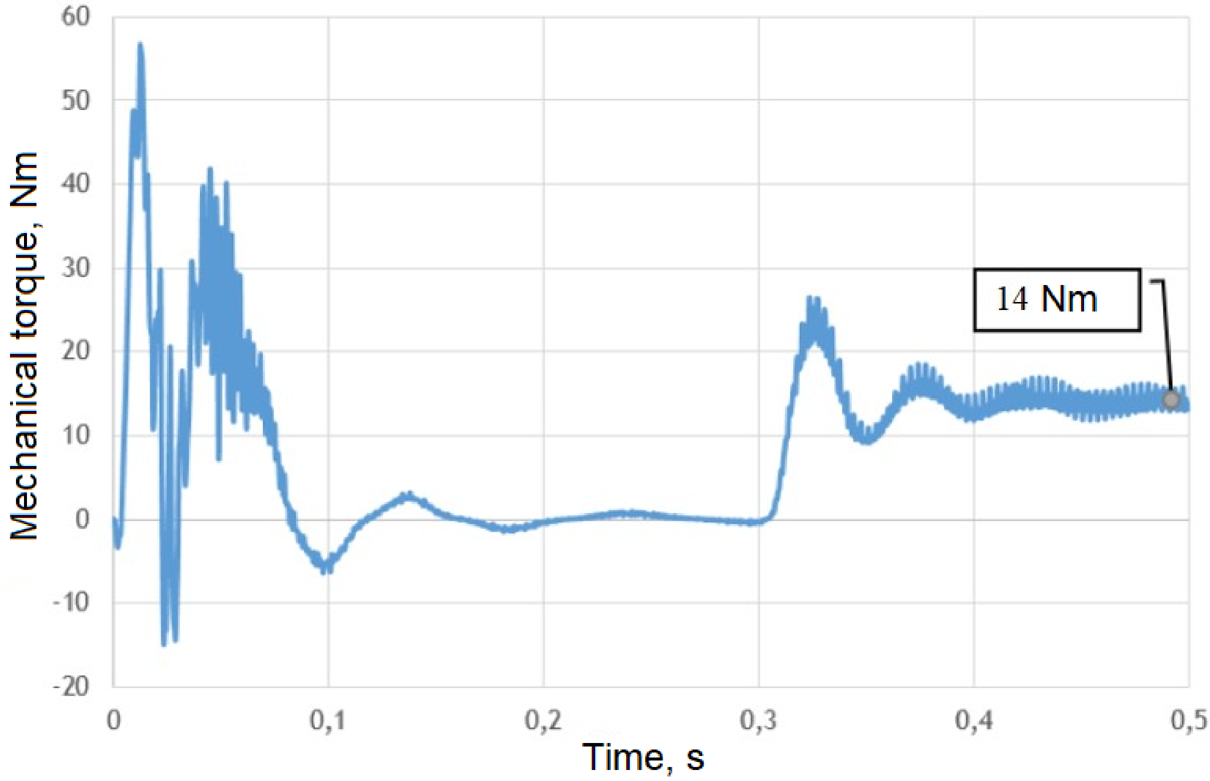

Figure 3.14 Mechanical torque of the motor

The graph of mechanical power is similar to that of mechanical torque. Figure 3.15 shows that the mechanical power has a high value at the beginning and then becomes zero at idle.

However, it has not yet stabilised, so some ripple can still be seen when the motor is idling, although the value when stabilised will be approximately 90W.

After 0.3 seconds, the motor starts to run under rated load conditions, and as expected, the mechanical power at this point is approximately 2.1 kW.

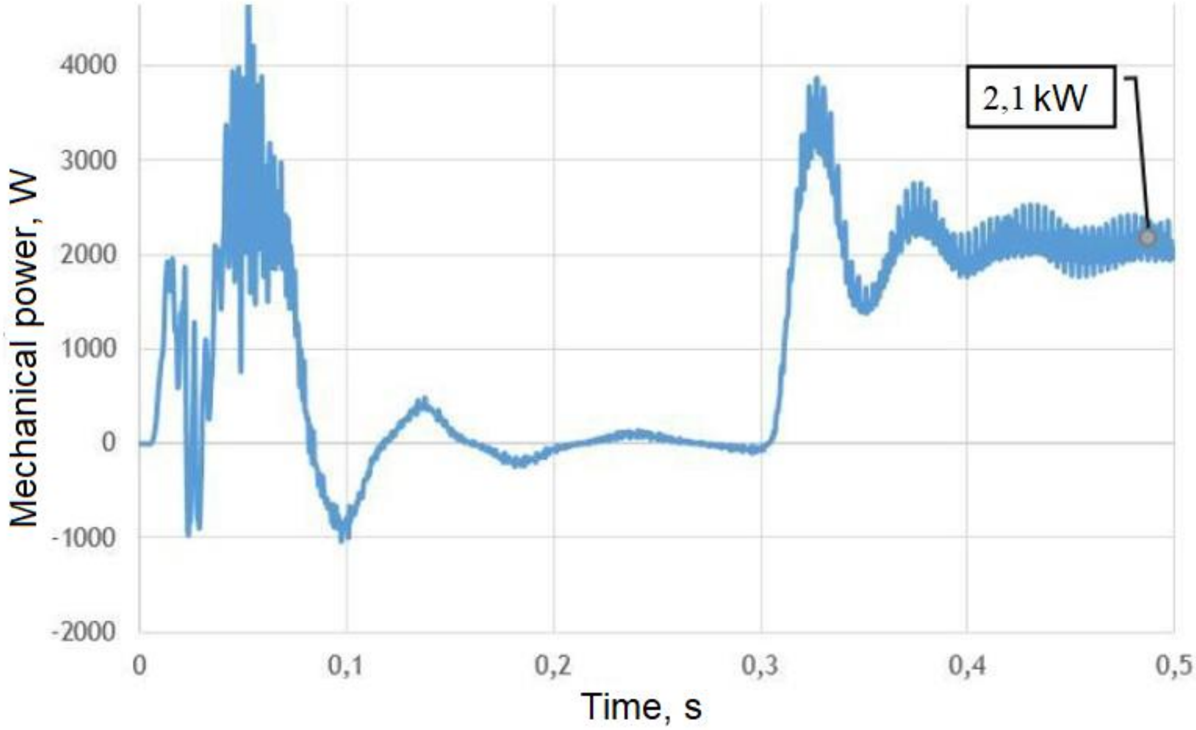

Figure 3.15 Mechanical power

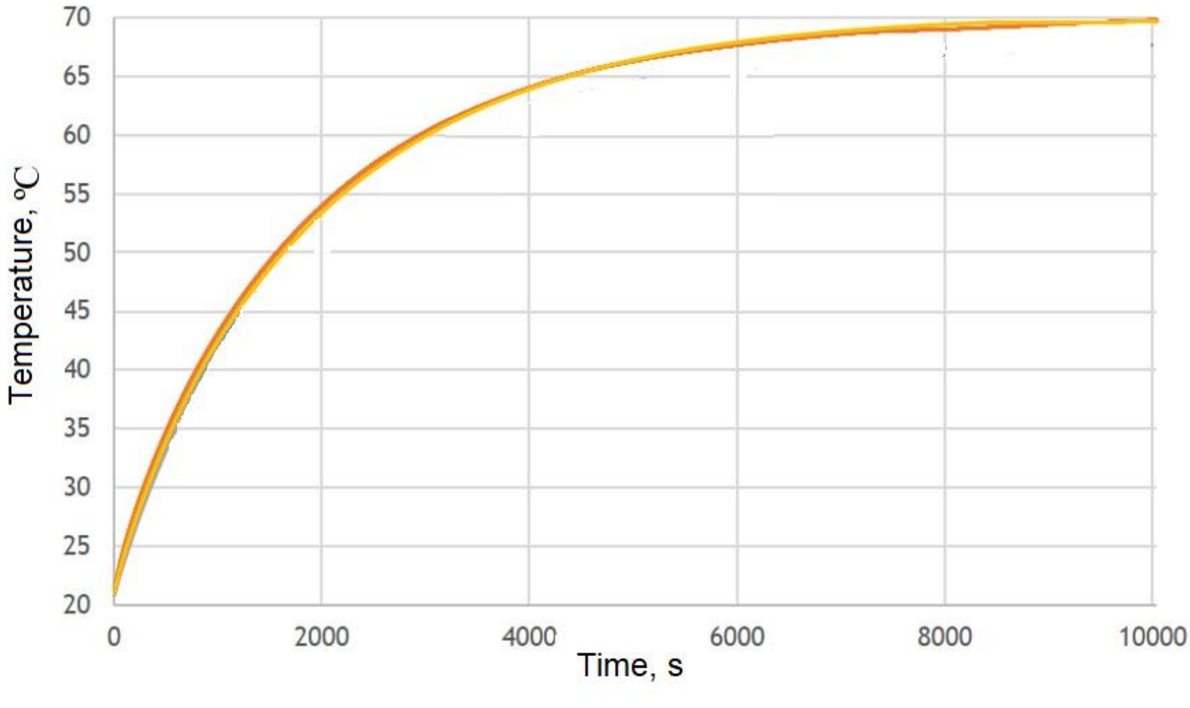

Figure 3.16 Motor rotor temperature

Figure 3.16 shows the motor rotor temperature curve obtained during the simulation for 10,000 seconds. It can be seen that the temperature increases rapidly during the first 1.5 hours. It reaches a value of 67 °C. Subsequently, the temperature remains virtually unchanged and does not exceed 75 °C.

3.5 Conclusions to the section

1. As a result of modelling and calculations, it was found that at the nominal slip value s = 0.04, the current in the windings is 4.56 A and the mechanical power is 14 N-m.
2. It is shown that the total losses in the motor are 158.21 W, of which the hysteresis losses and eddy current losses are 23.8 W.
3. The temperature calculation showed that in the loaded mode, the maximum rotor temperature does not exceed 80 °C. This temperature will not lead to a change in the electromagnetic characteristics of the motor elements when it is operated at an ambient temperature not exceeding 40 °C.

4 LABOUR OCCUPATIONAL SAFETY AND SECURITY IN EMERGENCY SITUATIONS

4.1 Effects of electromagnetic radiation on the human body

Electromagnetic radiation can be classified into two types: ionizing radiation and non-ionizing radiation, based on the capability of a single photon with more than 10 eV energy to ionize oxygen or break chemical bonds. Ultraviolet and higher frequencies, such as X-rays or gamma rays are ionizing, and these pose their own special hazards: see radiation and radiation poisoning. The electric currents that flow through power sockets have associated line-frequency electromagnetic fields. Various kinds of higher-frequency radio waves are used to transmit information – whether via TV antennas, radio stations or mobile phone base stations. By far the most common health hazard of radiation is sunburn, which causes over one million new skin cancers annually.

Before understanding electromagnetic radiation health effect to a human body, one must know how body cells function. In a human body, there is subtle electrical activity similar to electric circuits. This electrical activity controls vital bodily functions such as growth, metabolism, thought and movement. Body electrical currents are as critical to the well-being of human body as the flow of blood. Disturbance in this electrical network can be devastating to the correct and effective functioning of all organ systems, especially the brain. It is a health hazard and may lead to development of cancer and other diseases.

Modern technology uses a lot of electrical and field energies. Mobile phones, phone masts, power lines, wireless networks are all human technologies that involve field-effects. All these technologies use the electromagnetic spectrum. All energy, in fact, exists somewhere on that spectrum, including visible light, micro waves, and dangerous high-energy gamma radiation. Some people fear the effects of electromagnetic radiation on the human body.

There are some possible effects of Electromagnetic Fields (EMF) on Human Health under worst case conditions, i.e. at the highest power level, e.g., 2 W peak power. Maximum local SAR values averaged over 10 gram of tissue range typically between 0.2 and 1.5 W/kg, depending on the type of mobile phone. It has to be taken into account that the emitted power is often orders of magnitude lower than the maximum power leading to much lower exposure due to power control and several industrial appliances are operated in the RF and microwave range, for example for heating. The exposure of the worker operating such systems can reach values close or even above the limits.

Effects no a human body: human bodies are sensitive to even weak electromagnetic radiation. For example, low frequency electromagnetic radiation can affect a body's circadian rhythms. It affects the production of melatonin hormone, which is produced by brain's pineal gland. Melatonin is a hormone that regulates the biological rhythms of mammals. Research done at Battelle Pacific Northwest Labs has documented that prolonged exposure to electromagnetic radiation causes reduced melatonin secretion. Reduction of melatonin level threatens your health and can result in psychiatric disorders like depression, shortened attention span and inability to sleep. Decreased melatonin production can also increase the permeability of "blood-brain barrier", leaving a person even more vulnerable to chemicals toxic effects. Blood-brain barrier is a kind of safety barrier nature has provided human being to prevent dangerous molecules from entering the brain and causing damage.

A human body is protected by Blood-brain barrier: When a person is exposed to chemicals that find its way inside your bodies, two protective mechanisms are utilized. Melatonin neutralizes the free radicals (cancer-causing agents) created by the chemicals. And the blood-brain barrier prevents chemicals from entering the brain and spinal cord. Exposure to electromagnetic radiation breaks down the blood-brain barrier and hinders this protective mechanism.

Table 4.1 - Typical sources of electromagnetic fields

Frequency range	Frequencies	Field source	Examples of maximal intensities
Static	0 Hz	Natural VDU (video displays) MRI and other diagnostic / scientific instrumentation Industrial electrolysis	- 70 μT - 1 T in the tunnel; 200 mT at the gate; < 0.5 mT outside the device room 10-30 mT at the level of the feet
Extremely low frequency (ELF):	0-300 Hz 50 Hz	Powerlines Domestic distribution Electric engines in cars, train and tramway	- 10-20 μT under the line, or 10 kV/m - < 0.1-0.2 μT (microteslas) in the room - 50 μT and 300 V/m
Intermediate Frequencies	300 Hz – 100 kHz	Typical examples are: VDU, anti-theft devices in shops, hands free access control systems, card readers and metal detectors	- 30 to max 700 nT 10 V/m
Radio Frequency	100 kHz – 300 GHz	Broadcasting and TV; mobile telephony microwave oven Radar, portable and stationary radio transceivers, personal mobile radio.	- W/m² - 0.5 W/m² - 0.2 W/m²

It will also affect the permeability of cell membrane of a person's nerves, blood vessels, skin, and other organs. The intricate chromosomes DNA has also been shown to be affected by electromagnetic field. And iron, necessary for healthy blood and is stored in brain, is highly affected by electromagnetic radiation too.

Although electronic devices and the development in communications makes the life easier, it may also involve negative effects. These negative effects are particularly important in the electromagnetic fields in the Radiofrequency (RF) zone which are used in communications, radio and television broadcasting, cellular networks and indoor wireless systems. Along with the widespread use of technological products in daily life, the biological effects of electromagnetic waves has begun to be more widely discussed. The general opinion is that there is no direct evidence of hazardous effects on human health incurred by low-frequency radiofrequency waves. Studies at the cellular level, which uses relatively higher frequencies, demonstrate undesirable effects. In recent years there are a lot of studies about effects of EMF on cellular leve l; DNA, RNA molecules, some proteins, and hormones, intracellular free radicals, and ions are shown.

Particularly, the dramatically increasing number of mobile phones users rise significant concerns due to its potential damage on people exposed by radiofrequency waves. There are increasing number of in vivo, in vitro, and epidemiologic studies on the effects of mobile phones, base stations and other EMF sources in last decade.

Epidemiologic evidence compiled in the past ten years starts to indicate an increased risk, in particular for brain tumor, from mobile phone use. Because of mobile phones used close the brain tissue, electromagnetic waves affects it the most. The magnitude of the brain tumor risk is moderate.

A literature search on 'mobile phone use and cancer 'in PubMed lists 350 studies. More than half of all of these studies is related to brain tumors. At present, evidence for a causal relationship between mobile phone use and brain tumors

relies predominantly on epidemiology, in particular on the large studies on this subject. However, the etiopathogenesis of this causal relationship is not clear. The absence of this clear etiology even raise doubts about the cause itself. Weak evidence in favor of a causal relationship is provided by some animal and in vitro studies, but overall, genotoxicity assays, both in vivo and in vitro, are inconclusive to date.

4.2 Causes of electrical, voltage step

When a fault occurs at a tower or substation, the current will enter the earth. Based on the distribution of varying resistivity in the soil (typically, a horizontally layered soil is assumed) a corresponding voltage distribution will occur. The voltage drop in the soil surrounding the grounding system can present hazards for personnel standing in the vicinity of the grounding system. Personnel “stepping” in the direction of the voltage gradient could be subjected to hazardous voltages. In the case of Step Potentials or step voltage, electricity will flow if a difference in potential exists between the two legs of a person. Calculations must be performed that determine how great the tolerable step potentials are and then compare those results to the step voltages expected to occur at the site. During an interruption relation to the ground (ground fault), an electric current flowing through the grounding system to ground rod or other grounding system (the metal structure, grounding wire) and returned to the source of electrical power. The possibility of electric current flow can occur along the ground at a certain distance around the point where the ground gets reinforcement or into voltage. Electrical current will follow in the section closest to the fault current drain conductors.

Voltage step (step potential) caused by the flow of fault current through the ground. The closer the personnel with a ground rod or a grounded device, the greater the concentration of flows and the greater the voltage or electric potential. The flow of electrical current creates a voltage drop (voltage drop) because of the electric current flowing through the ground and the person or personnel maintenance stand with wide footfall such as shown in Figure 1.6, becomes part of the bridge of a voltage drop that creates a path parallel to the flow of electric current,

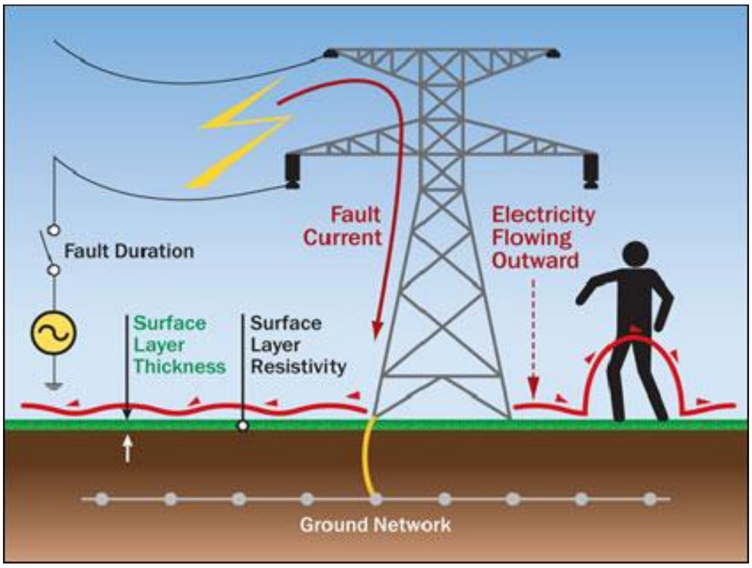

Figure 4.1 - The Step Voltage by a personnel maintenance

The larger the width of footsteps personnel, the greater the voltage difference is perceived by the personnel. To protect themselves or to avoid danger to personnel exposed to a voltage step that is being worked on equipotential zone, can do the best defense is simple: always be wary of any step voltage.

Hazardous Step Potentials or step voltage can occur a significant distance away from any given site. The more current that is pumped into the ground, the greater the hazard. Soil resistivity and layering plays a major role in how hazardous a fault occurring on a specific site may be. High soil resistivities tend to increase Step Potentials. A high resistivity top layer and low resistivity bottom layer tends to result in the highest step voltages close to the ground electrode: the low resistivity bottom layer draws more current out of the electrode through the high resistivity layer, resulting in large voltage drops near the electrode. Further from the ground electrode, the worst case scenario occurs when the soil has conductive top layers and resistive bottom layers: in this case, the fault current remains in the conductive top layer for much greater distances away from the electrode. Fault clearing time is an important factor to consider as well. The more time it takes the electric utility company to clear the fault, the more likely it is for a given level of current to cause the human heart to fibrillate.

An important note to remember is that most power companies use automated re-closers. In the event of a fault, the power is shut off and then automatically turned back on. This is done in case the faults occurred due to an unfortunate bird that made a poor choice in where to rest, or dust that may have been burned off during the original fault. A few engineers believe that Fibrillation Current for Step Potentials must be far greater than Touch Potentials, as current will not pass through any vital organs in the former case. This is not always true as personnel that receive a shock due to Step Potentials may fall to the ground, only to be hit again, before they can get up, when the automatic re-closers activate.

GENERAL CONCLUSION

1. It has been shown that in electric motors, the thermal and electromagnetic fields are interconnected and directly affect its design. Among the existing modeling methods, a numerical method for calculating the field based on the finite element method was chosen.

2.The mathematical models for calculating electromagnetic and thermal fields are presented, which allow determining losses in motors and temperatures of its elements, both in the stationary and transient processes.

3.The analysis shows the importance of taking into account the temperature change in winding resistance when constructing thermodynamic models of electric machines. It is shown that the change in the winding temperature will be insignificant within the cycle, but the average temperature level of the model nodes will significantly depend on the fact of taking into account the temperature change in resistance. In most cases, the temperature dependence of the thermal conductivities and heat capacities of copper and aluminum can be ignored. Ignoring the temperature dependence of the thermal conductivities of air and steel, as well as the heat capacity of iron-containing motor elements, can lead to significant calculation errors.

4.The geometry of the model of an induction motor with a squirrel-cage rotor was developed in the FluxMotor program based on its data sheet. A finite element mesh was constructed and electrical and magnetic parameters of materials were assigned to the model elements.

LIST OF REFERENCES

1. Elektrychni mashyny i aparaty: navchalnyi posibnyk / Yu.M.Kutsenko, V.F.Iakovliev ta in.–K.: Ahrarna osvita, 2013. –449 s

2. Kral, M., & Gono, R. (2017, May). Dynamic model of asynchronous machine. In 2017 18th International Scientific Conference on Electric Power Engineering (EPE) (pp. 1-4). IEEE.

3. Zalizetskyi A.M. Doslidzhennia chastotnoho elektropryvoda v statychnykh rezhymakh roboty /A.M. Zalizetskyi, O.V. Pizniur // Visnyk Khmelnytskoho natsionalnoho tekhnichnoho universytetu. – Khmelnytskyi: KhNU, 2012. – № 3. – S. 69-74.

4. Boldea, I. (2020). Induction Machines Handbook: Transients, Control Principles, Design and Testing. CRC press.

5. Ovcharenko V.A., Podliesnyi S.V., Zinchenko S.M. Osnovy metodu kintsevykh elementiv i yoho zastosuvannia v inzhenernykh rozrakhunkakh: Navchalnyi posibnyk. – Kramatorsk: DDMA, 2008. – 380 s

6. Müller, T., Blazek, G., & Henning, F. (2016). Design concept of a lightweight electric motor casing with support from thermomechanical simulations. International Journal of Automotive Composites, 2(2), 167-186.

7. Stopin Yu. O. Matematychna model teplovykh protsesiv asynkhronnykh elektrodvyhuniv pry nesymetrii napruh //Visnyk Kharkivskoho natsionalnoho tekhnichnoho universytetu silskoho hospodarstva imeni Petra Vasylenka. – 2015. – №. 165. – S. 128-129.

8. M. Bose, A. Bhattacharjee, and R. Sudha, “Calculation of induction motor model parameters using finite element method,” International Journal of Soft Computing and Engineering (IJSCE), vol. 2, no. 3, pp. 41–43, 2012.

9. Zubenko D. Yu., Petrenko O. M. Teplova i elektrychna matematychna model dlia asynkhronnykh elektrodvyhuniv //Komunalne hospodarstvo mist. – 2019. – №. 149. – S. 16-18.

10. Flux Leading Software for Electromagnetic and Thermal Simulations: http://www.cedrat.com/software/flux/

11. Adouni, A.; Cardoso, A.J.M. Thermal analysis of low-power three-phase induction motors operating under voltage unbalance and inter-turn short circuit faults. Machines 2020, 9, 2.

12. Xie, Y.; Wang, Y. 3D temperature field analysis of the induction motors with broken bar fault. Appl. Therm. Eng. 2014, 66, 25–34.

13. Kostiaieva M. S. Vymohy bezpeky pid chas ekspluatatsii elektrodvyhuniv vlasnykh potreb //BBK 74.58 I-66. – 2016. – S. 88.

14. Automation & Motors European Product Lines [Електронний ресурс] – Режим доступу : https://www.weg.net/institutional/UA/en/

15. Коваль В.П. Методичні вказівки до виконання кваліфікаційної роботи магістра для здобувачів другого рівня вищої освіти за ОПП Електроенергетика, електротехніка та електромеханіка/ В.П. Коваль, М.Г. Тарасенко, О.А. Буняк, Л.Т. Мовчан – Тернопіль: ТНТУ, 2024. – 51 с.